Proceedings


Czech and Slovak Society for Photonics

Czech Technical University in Prague, Faculty of Electrical Engineering

Action M Agency

# OPTICAL COMMUNICATIONS 2019

**November 11–12, 2019, Prague, Czech Republic**

Edited by: Jiří Vodrážka

Published by:
Zeithamlová Milena Ing., Agentura Action M
Vršovická 68, 101 00 Praha 10, Czech Republic

ISBN: 978-80-86742-52-6

# 30th Conference and Exhibition on Optical Communications 2019 Proceedings

November 11-12, 2019, Prague - Czech Republic

## Conference Topics

- Technologies, design and services of NGN/NGA
- Photonic technologies for Industry 4.0
- Optical networks for Smart Grid
- Optical transmission systems and network elements
- Optical fibres, cables and components
- Planar optical and optoelectronic integrated components
- Passive and active components - their production and testing
- Fibre lasers
- Installation, measurement, diagnostics and maintenance of optical cables
- Optical fibre sensors
- Optical signal processing
- Organic materials for optics and optoelectronics
- Optical nano-waveguides
- Free-space optical signal transmission (FSO)
- Biomedical applications of fibre optics and optoelectronics

## Sponsored by

- Czech and Slovak Society for Photonics
- Czech Technical University in Prague, Faculty of Electrical Engineering

*Edited by:* Jiří Vodrážka and Stanislav Zvánovec

*Published and produced:*
Zeithamlová Milena Ing., Agentura Action M, Vršovická 68, 101 00 Praha 10
actionm@action-m.com



**ISBN: 978-80-86742-52-6**

## About the Conference

The papers included in these proceedings were presented at the 30th Conference and Exhibition on Optical Communications 2019 (OK 2019) organized by the Czech and Slovak Society for Photonics, Faculty of Electrical Engineering of the Czech Technical University in Prague and Action M Agency. Traditionally, the conference was held in the beautiful historic city, the capital of the Czech Republic.

In the third decade, the conference continues the successful editions of OK conferences established by pioneer Czech optical researchers in mid-eighties. The main objective is to offer an international forum for the exchange of new ideas, thoughts, and realizations on physics, technologies, and applications of optics. Even though it is impossible for the conference to cover the entire area of optical communication technology as it is intensively developing these days, it tries to focus on vivid topics of the theory and applications that have a significant impact on our society's everyday life. Traditionally, the conference offers an excellent opportunity for young scientists to present their recent research results.

We want to thank the volunteers who helped us to attract high-quality contributions, all those who submitted papers for review and those who provided manuscripts for publication in these proceedings. We also wish to sincerely thank the members of OK 2019 committees, our partners who supported this event, and everyone who helped to organize the conference.

Jiří Vodrážka and Stanislav Zvánovec

Czech Technical University in Prague, Faculty of Electrical Engineering

## Scientific Committee

**Chairman:**

Jiří Vodrážka, FEE CTU in Prague, Czech Republic

**Members:**

- Leoš Boháč, FEE CTU in Prague, Czech Republic
- Jan Brouček, PROFiber Networking , Czech Republic
- Pavel Černý, SITEL, Czech Republic
- Milan Dado, ZU Žilina, Slovak Republic
- Pavel Honzátko, Institute of Photonics and Electronics AS CR, Prague, Czech Republic
- Vítězslav Jeřábek, FEE CTU in Prague, Czech Republic
- Miloš Klíma, FEE CTU in Prague, Czech Republic
- Jaroslav Kováč, FEI STU Bratislava, Slovak Republic
- Petr Páta, FEE CTU in Prague, Czech Republic
- Jaromír Šíma, RLC Praha, Czech Republic
- František Uherek, FEI STU Bratislava, Slovak Republic
- Otakar Wilfert, FEEC BUT Brno, Czech Republic
- Stanislav Zvánovec, FEE CTU in Prague, Czech Republic

## Content of Conference Proceedings

# 40 years of technological research of optical fibers in Czech academical institutions

Vlastimil Matějec, Ivan Kašík

*Institute of Photonics and Electronics of the Czech Academy of Sciences, Chaberská 57, Prague 8*

***Abstract*— In this year, the anniversary of 40 years of technological research of optical fibers in Czech academic institutions is marked at the Institute of Photonics and Electronics of the Czech Academy of Sciences. This paper shows important results of this research achieved during these 40 years. The research has been carried out in Czechoslovak Academy of Sciences and Czech Academy of Sciences in close collaboration with the Czech Technical University and University of Chemistry, Prague. On the basis of optical fiber applications, this research can be divided into two main areas. In first area dated to years 1979-1990, the technology of fibers for telecommunications was mainly investigated. Approaches for the preparation of polymer-clad silica fibers, graded-index fibers and single-mode fibers were developed. In second area, i.e. in a period since 1991, the technology of fibers for fiber lasers, fiber-optic chemical sensors and energy delivery has been investigated. The paper presents some characteristics of such fibers, e.g. attenuation, dispersion, limit of detection, etc. as well as briefly describes the technology of their fabrication. It also reports references to papers in which results of this research have been published. Some, still unpublished results are given in the paper.**

***Index Terms*— Czech academy, optical fiber, properties, technological research.**

## I. INTRODUCTION

Silica optical fibers belong without doubts to technical means that have substantially contributed to the rapid progress in telecommunications within last 50 years [1]. Such progress is closely connected with the development of technology for their preparation [2]. First steps of this development in world can be dated to 70's of the last century. It is useful to mention that E. Spitz, who had graduated from the Czech Technical University (CVUT), Prague, highly contributed to this world development working in Thomson-CSF, France in that time. Optical fibers investigated by Thomson-CSF were fabricated from multicomponent glasses and exhibited high losses about 3dB/m [3]. Further progress in the optical fiber development is related to an article of K.C. Kao and G.A. Hockmann from Standard Telecommunication Laboratories Ltd., England. In their article, they predicted that optical fibers with a losses of about 20 dB/km could be produces from fused silica with an iron content below $10^{-8}$ mol.% [4]. This prediction paved the way for the optical fiber technology and K.C. Kao received for it one half of Nobel Prize in Physics in 2009. In agreement with this prediction, first silica step-index fibers doped in the core with titanium dioxide with losses of about 16 dB/km were drawn at Corning Glass, USA in 1970 [1]. Preforms of such fibers were fabricated by chemical vapor deposition.

Such progress was also reflected in Czechoslovakia. In 1977, J. Gotz from the Joint Laboratory for Chemistry and Technology of Silicates of the Institute of Chemical Technology (ICT), Prague and Czechoslovak Academy of Sciences (further on abbreviated as SLS,) invited P. Schulz from Corning Glass to XI. World Congress on Glass of ICG with a lecture on glass as medium for transmitting information. Shortly after the congress it was decided officially that Czechoslovak Academy of Sciences (CSAV) and particularly SLS will deal with the research of technology of optical fibers, i.e. with investigations of materials and processes for the optical fiber preparation. This research started in 1979, i.e. 40 years ago. In this paper we would remind important results of this technological research achieved during this 40-year period and present also some so far unpublished results on optical fibers developed in this research.

## II. PERIOD 1979-1990 - FIBERS FOR TELECOMMUNICATIONS

### *A. Joint Laboratory for Chemistry and Technology of Silicates*

In 1979, a governmentally supported research project called "Optical Waveguides-Preparation" and focused onto investigation of technology of silica optical fibers began in SLS. The project was solved in laboratories of SLS located at Sokolska 38, Prague 2, At starting stages of this project in 1979 suitable technology of silica fiber fabrication was identified on the basis of available information and devices for its realization were designed by a group of researches including J. Götz, G. Kuncová, J. Kynčl, M. Pospíšilová, This technology consisted of the Modified Chemical Vapor Deposition (MCVD) for the fabrication of fiber preforms and of a fiber drawing from such preforms at temperatures around 2000 °C. A laboratory MCVD device (further on called MCVD I) and fiber-drawing tower were constructed in 1980. Such set ups were based mainly on production of Czechoslovak companies with the exception of a graphite resistance furnace Centorr installed at the drawing tower and imported from USA. It is remarkable that this furnace is operated till now thanks to spare graphite heating elements developed within the collaboration of SLS and Elektrokarbon, Topolcany in 1985.

By using MCVD I device, technology of step-index (SI) and graded-index (GI) fibers was investigated by V. Havranek, Z. Choc, J. Kynčl, V. Matějec in a period 1981-1986. Fibers doped in the silica core with germanium dioxide and phosphorus pentoxide and with silica cladding doped with boron oxide and later on with fluorine were prepared

[5],[6]. Such fibers were designed for operating at first telecommunication window, i.e. at a wavelength of 850 nm. Samples of fibers with optical losses of 2.8-4 dB/km and bandwidths of 50-90 Mhz.km for SI fibers and 400-700 Mhz. km for GI fibers were usually prepared at SLS in 1986 [6]. It is necessary to notice that the MCVD technology profited from the availability of silicon tetrachloride (quality FO Optipur) that was purified on the basis of a method developed by D. Ležal and M. Pedlík [7]. This method enabled concentrations of impurities to be decreased below $10^{-8}$ mol.%. On its basis the production of FO Optipur silicon tetrachloride was realized at Tesla Rožnov.

The developed drawing tower was employed for drawing fiber samples from preforms produced on MCVD I device. Moreover, a group including M. Hayer, M. Hrabalová, G. Kuncová, S. Schätz dealt with the technology of polymer-clad silica (PCS) fibers in 1981-1985. These fibers were drawn from high-quality silica rods Suprasil (Heraeus, Germany) and employed optical cladding of polysiloxane polymer (imported from France, Japan, USA). Fiber samples with optical losses of 11 dB/km at around 850 nm and with a sufficient mechanical strength [8] were regularly prepared at SLS in 1984. With such fibers, first public signal transmission through Charles bridge, Prague was presented on Czechoslovak TV on July 4th, 1984. The technology was proved on production of more than 50 km of PCS fibers in SLS and then transferred into a pilot plant production at a Research Institute of Sklounion (VUSU) Teplice.

Laboratory set ups and methods for the characterization of optical losses and refractive-index profiles of prepared fibers were also developed in SlS by M. Pospíšilová, J. Veselý in close collaboration with the Faculty of Nuclear Sciences and Physical Engineering (FJFI), CVUT, Prague and with the Institute of Radio Engineering and Electronics (URE), CSAV, Prague. The cut-back method was regularly used for spectral attenuation measurements [9]. At beginning, refractive-index profiles of preforms and fibers were reconstructed from electron microprobe measurements of dopant concentrations carried out by V. Hulinský. Latter on a laboratory set up was developed for the refractive-index profile measurements at FJFI.

In 1986 new laboratories of SLS were opened in a new building constructed at Prague 6-Lysolaje, Rozvojová 135. These laboratories were equipped with a commercial MCVD device (further on called as MCVD II) from Special Gas Control, Great Britain, and Arnold Ltd., Germany. The fiber-drawing tower was transferred into these laboratories from the drawing laboratory of SLS at Sokolská 38, Prague 2. Moreover, characterization laboratories with a commercial refractive-index profilers and optical losses measuring device purchased from York Technology, Great Britain. In 1987, SLS was transformed into the Institute of Chemistry of Glass and Ceramic Materials (ICGCM) of CSAV in order to further support the technological research of optical fibers.

### *B. Institute of Chemistry of Glass and Ceramic Materials*

In a period 1986-1990, the investigation of the preform technology took place both in laboratories in Rozvojová 135 and Sokolská 38. In the latter place, a team consisting of V. Matějec, N. Novotná, M. Sedlář, S. Poláková continued with preform preparations on the device MCVD I. In 1986, research activities were focused on the processes for the preparation of fiber claddings doped with fluorine [10]. In 1986-1988, the technology of single-mode (SM) fiber preparation was developed. Preforms for drawing different types of these fibers were fabricated [11]. Fiber samples with optical losses 0.5 dB/km and dispersion -3.5 ps/(nm.km) at 1300 nm were obtained. Such parameters were comparable with commercially available SM fibers operating at this telecommunication window in that time.

In years 1988-1990 the team focused on the technology of optical fibers doped in the core with rare-earth ions such as neodymium and erbium ones. For such purpose, the solution doping method reported by D. Payne et al. in 1986 [12] was implemented. The method employed soaking a silica frit prepared during the MCVD deposition inside a silica tube with a aqueous solution of erbium or neodymium salts. The soaked frit was then sintered into a glass layer from which a preform core was formed during the collapse of the tube to a rod, the preform. Different fibers with erbium- and neodymium-doped fiber cores were prepared with maximum rare-earth concentrations of about 0.06 mol.% and bas-line losses around 60 dB/km [13]. On the basis of such fibers a first Czechoslovak erbium fiber laser emitting at 1550 nm was developed in URE CSAV in 1990.

The research team working with the device MCVD I in collaboration with a team of G.A. Ivanov from Institute of Radio Engineering, Academy of Sciences of USSR, Moscow, developed also original technology for the fabrication of polarization maintaining “bow-tie” fibers. This technology employed thermal screens fixed to a deposition tube inside which a stress layer doped with boron oxide and applied during the MCVD process was etched by fluorine under the tube rotation [14]. Fibers with beat lengths of about 5 mm at 1000 nm were drawn from such preforms. After social changes in 1989 it was decided to stop working on the device MCVD I. The device was dismantled in 1990.

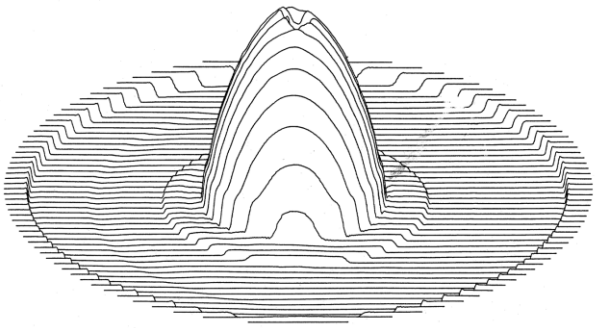

Fig. 1 Typical tomographic refractive-index profile of a GI fiber preform fabricated at ICGCM; core diameter of 4.9í mm, core-cladding refractive-index difference of 0.016

### *C. Technological Research at the novel laboratories in Prague 6*

In years 1986-1990, a team of M. Hayer, Z. Choc, I. Kašík, K. Matějovič, O. Sysala, J. Zátorský working in the new building in Rozvojova 135 further developed the technology of GI fibers for a wavelength of 850 nm (see a refractive-index profile of a preform in Fig. 1) [15]. These fibers had GI cores with a diameter of 50 μm which were prepared of silica doped with germanium dioxide and phosphorus

pentoxide. Fiber claddings were of silica doped with fluorine and small amounts of phosphorus pentoxide. This technology was proved by the pilot plant production of such GI fibers in ICGCM. More than 300 km of such fibers was fabricated in a period 1986-1988. Prepared preforms and fibers were immediately characterized by M. Pospíšilová and A. Spáčilová. The statistical evaluation of measured results showed that 65% of these fibers had losses lower than 3 dB/km [15]. Bandwidth values were between 200-500 Mhz.km for 46% of the prepared fibers, and of 500-800 MHz.km for 45% of fibers. Such results were in a full agreement with regulations of the International Commission of Electronics and they were fully comparable with parameters reported by world GI fiber producers. During years 1988 and 1989, the GI fiber technology was transferred into the pilot plant production at VUSU Teplice. Subsequently, the research of the technology of SM fibers for a wavelength of 1300 nm and their pilot plant production were carried out in ICGCM. As in 1990 it was officially decided not to invest into industrial manufacturing of optical fibers for telecommunications in Czechoslovakia, the research of the technology of optical fibers in ICGCM was further focused on special optical fibers for sensors and lasers.

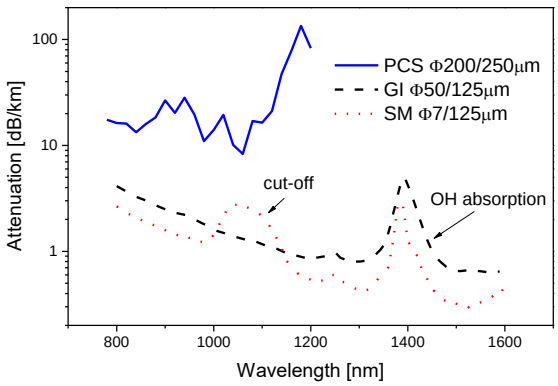


Fig. 2 Examples of spectral attenuation curves of fibers for telecommunications prepared in SLS and ICGCM

Results of the technological research of optical fibers reviewed above enable to conclude that in field of fibers for telecommunications an initial ten-year delay between this research in world and in Czechoslovakia was decreased to about three-year delay. As one can see from Figs. 1 and 2, this research resulted into preparation of optical fibers with spectral attenuation values comparable with those of world producers in that time. Fibers fabricated in SLS and ICGCM were employed for test experiments on the development of fiber cables in companies Kablo Bratislava and Kablo Děčín. They enabled also to develop procedures for fiber characterization techniques in VUSU Teplice. Thus, they contributed to creating experiences of staff dealing with such complex manufacturing activities.

## III. PERIOD SONCE 1991-TECHNOLOGY OF FIBERS FOR LASERS, SENSORS, ENERGY DELIVERY

### *A. Institute of Chemistry of Glass and Ceramic Materials*

The beginning of this period can be characterized by the concentration of all technological facilities for the optical fiber fabrication at the building in Rozvojová 135, Prague 6. By using these facilities, the technology for the preparation of silica optical fibers doped with rare-earth ions was further improved. In a period 1991-1992, an original doping approach was developed that was based on using solutions of rare-earth salts and aluminum chloride in organic solvents for the frit soaking [16]. Such an approach improved the frit drying. In the same period, polarization-maintaining "bow tie" fibers were also fabricated by using the developed gas-phase etching. Such fibers were tested in a fiber-optic gyroscope developed in URE CSAV.

### *B. Institute of Radio Engineering and Electronics and Institute of Photonics and Electronics*

In spring 1993, activities of ICGCM were finished by the decision of the Academic Assembly of CSAV. Researchers I. Kašík, and V. Matějec were transferred to URE CSAV together with the technological and measurement devices installed in the building in Rozvojová 135, Prague 6. Since that time, three main areas of the technological research of optical fiber fabrication can be recognized in URE, namely, optical fibers for fiber lasers and amplifiers, fibers for chemical sensors, and fibers for energy transfer. This research has profited from the close collaboration with researches J. Čtyroký, P. Honzátko, M. Chomát, J. Kaňka, P. Peterka dealing with design and characterization of optical fibers in URE and with O. Podrazký who has been investigating fiber-drawing technology. The technological research was further strengthen by installing a new fiber-drawing tower in 2000. In 2007, URE became a public research institute and it was renamed to the Institute of Photonics and Electronics (UFE) of the Czech Academy of Sciences.

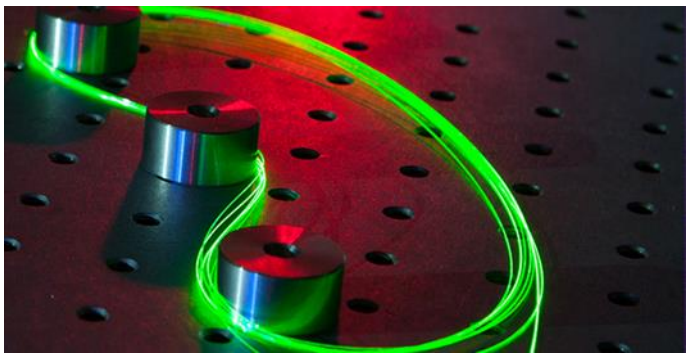

Fig. 3. Photo of a laboratory setup of a highly efficient laboratory Tm fiber laser pumped at 1600 nm; intensive green up-conversion radiation irradiated from the fiber proves a high laser efficiency around 1900 nm

The research of the technology of optical fibers for lasers was focused onto issues such as suitable matrices suppressing clustering of rare-earth ions, new rare-earth dopants. Thus, original approaches for the preparation of silica cores doped with aluminum oxide and high content of phosphorus pentoxide developed in URE enabled us to increase concentrations of rare-earth dopants and decrease base-line fiber losses. By using these approaches, optical fibers doped in the core with erbium and ytterbium ions were prepared which enabled to setup very efficient high power laboratory lasers emitting around 1550 nm when pumped at 1060 nm. These lasers were successfully tested for generating ultrashort

soliton pulses around 1995 [17]. Recently, optical fibers doped in the core with thulium ions have been fabricated by developing original approaches employing nanoparticles during the fabrication [18]. Lasers based on such fibers operate at wavelengths around 2000 nm when pumped at 1600 nm (see a laboratory set up in Fig. 3). The possibility of achieving the longer lasing wavelengths is investigated now by the development of fibers doped in the core with holmium.

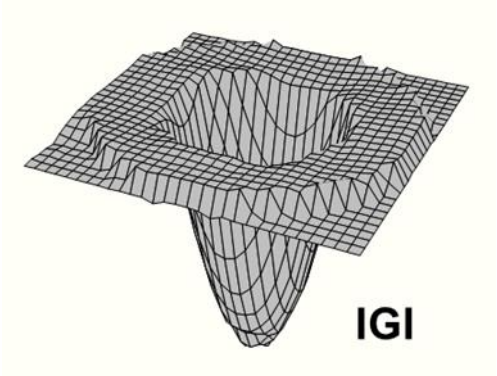


Fig. 4 Tomographic refractive-index profile of a sensing fiber with an inverted-graded index (IGI) profile of the core; core diameter of 250 μm.

Large effort was focused to the development of approaches for the fabrication of optical fibers for evanescent-wave chemical sensing in a period 1994-2000. Such fibers relayed on beveled or U-shaped PCS fibers, special- shaped sectorial fibers prepared from multimode step-index fibers, original multimode fibers with inverted-graded refractive-index profiles (see Fig. 4), fiber tips , etc.[19]-[21]. All these fibers enabled us to increase the fraction of power transmitted in the evanescent-wave area and thus to increase the response and detection sensitivity. Such fibers were tested for the detection of aromatic hydrocarbons in water with a detection limit below 5 mg/l, or for pH measurements. For such detection, special porous membranes were applied by the sol-gel method onto the fibers [20].

On the basis of such results, URE researchers were invited to participate in an EC-supported project MATINOES (2002-2005) and together with K. Rose (Institute for Silicate Research, Germany), N. Jaffrezic-Renault (CNRS France), L. Šašek (Safibra,s.r.o., Říčany, CR) and others develop fiber-optic oxygen and glucose sensors for food processing [21]. Moreover, UFE researchers participated at a Czech Center of Excellence REMOROST supported by Ministry of Education, Youths, and Sport, CR and coordinated by E. Zažímalová (Institute of Experimental Botanic AS CR, Prague) in a period 2006-2011. In this Center, they investigated a sensor for pH detection in plants. The sensor was based on fiber tips coated by a suitable pH transducer immobilized in a porous layer. It was tested for pH detection in small drops of plant exudates [22]. It is necessary to mention that a prototype of such a sensors has been developed in the collaboration with Safibra, s.r.o., recently.

In years 2012-2018, the technology for the fabrication of microstructured fibers (MSFs) and Bragg fibers was also investigated in UFE MSFs were drawn from preforms fabricated by the stack and draw technique. Such a technique employed a stack composed of a central silica rod surrounded by arranged silica capillaries and placed into an outer jacketing silica tube. This investigation was carried out in the collaboration with FJFI CVUT. Different MSFs were fabricated in a period 2002-2007 (see an example of the cross-section in Fig. 5). They were tested in evanescent-wave oxygen and toluene sensors [23].

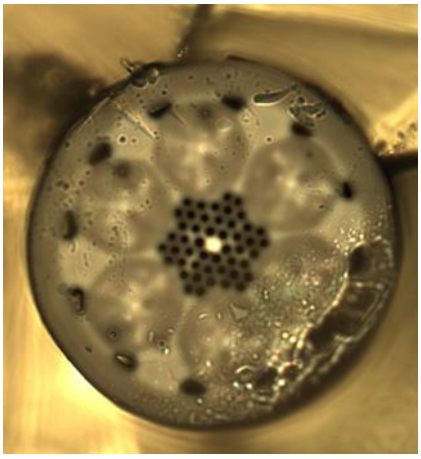

Fig. 5. Microscope cross-section of a microstructured with a silica core and the cladding of silica and air holes showing light confining into the core; outer fiber diameter was 125 μm, core diameter of 5.5 μm

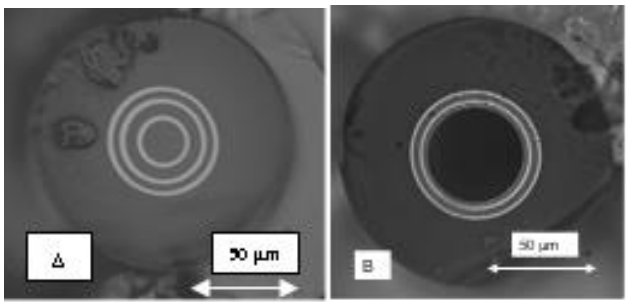


Fig. 6 Microscope cross-sections of Bragg fibers; A) fiber with a silica core, B) fiber with a hollow-core

Bragg fibers (see Fig. 6) with silica cores and hollow cores and with claddings of three pairs of alternating high- and low-index layers were drawn from preforms fabricated by the MCVD method. The high-index layers (bright ones in Fig. 6) were prepared of silica doped with germanium dioxide. Such fibers were tested for delivery of laser radiation at 1060 and 1940 nm [24]. High damage thresholds of about 30 GW/cm$^2$ and minimum losses of about 0.1 dB/m of these fibers were determined.

## IV. CONCLUSION

The review on the investigation of fiber-optic technology and its results presented above enable us to draw several conclusions. Thus, the review shows that Czech researchers and technicians have been capable to manage such complex technology as the technology of silica optical fibers is. They designed and set up laboratory devices for MCVD preform fabrication, fiber drawing and characterization in starting years of the research from 1979 to 1986 only on the basis of information in literature. Fiber samples produced on these devices had characteristics comparable with those reported in world. After that, they mastered new commercial devices and employed them for laboratory and pilot plant preparations of GI and single-mode fibers for telecommunications in years

1986-1990.

Since 1991 they have been using their experience for developing fibers for fiber lasers, chemical fiber sensors and fibers for laser power delivery. Their original results enabled their involvement into important international and national research projects.

Unique research technological facilities installed in the building of UFE in Prague 6 make possible not only to carry out high quality material research of optical fiber technology, but they enable to show students and public visitors' basic steps of this technology. Thus, this research contributes both to knowledge in the field of technology and to education.

## ACKNOWLEDGMENT

The presented technological research could not be carried out without institutional financial support from Czechoslovak and Czech Academies of Sciences and without a number of grants from the Czech Science Foundation, Technology Agency of the Czech Republic, Ministry of Education, Youths, and Sports, CR. One project was supported by EC within the framework FP5. The authors would like to thank technicians included in the research, K. Jirák, V. Kolář, V. Janotková, A. Šturma, R. Vogt …, without whose experimental facilities for fiber preparation and characterization could not work.

## REFERENCES

[1] E. Desurvire, C. Kazmierski, F. Lelarge, X. Marcadet, A. Scavennec, F.A. Kish, D.F. Welch, R. Nagarajan, C.H. Joyner, R.P. Schneider, S.W. Corzinec, M. Kato, P.W. Evans, M. Ziari, A.G. Dentai, J.L. Pleumeekers, R. Muthiah, S. Bigo, M. Nakazawa, D.J. Richardson, F. Poletti, M.N. Petrovich, S.U. Alam, W.H. Loh, D.N. Payne, "Science and technology challenges in XXIst century optical communications," *C. R. Physique 12*, pp. 387-416, 2011.

[2] J. Hecht, *City of Light The Story of Optical Fibres*, Oxford University Press, New York, 2004, pp. 131-176.

[3] A. Werts, "Propagation de la lumiere coherente dans les fibres optiques", *L' Onde Electique XLVI, n°474*, pp. 967-980, 1966

[4] K.C. Kao and G.A. Hockham, "Dielectric-Fibre Surface Waveguides for optical frequencies," *in Proc. IEE 113*, pp. 1151-1158, 1966

[5] V. Havranek, Z. Choc, J. Gotz, V. Hulinsky, "Priprava preform pro celosklenena svetelna vlakna, *"in Sborník konference Optické komunikace 1984*, Praha, 1984, pp.. 18-22

[6] J. Götz, M. Hayer, Z. Choc, G. Kuncová, V. Matějec, "Laboratorní příprava světlovodných vláken typu SI a GI," *in Sborník konference Optické komunikace 1986,* Praha, 1986, pp. 18-22.

[7] D. Ležal, J. Doležal, M. Pedlík, "Problematika organosloučenin a hydridů při čištění SiCl4 pro optická vlákna," *in Sborník semináře Optické komunikace 1984*, Praha, 1984, pp. 28-29.

[8] S. Schätz, M. Hayer, G. Kuncová, V. Matějec, M. Hrabalová, "Vliv tažení na pevnost vláken typu PCS," *in* Sborník *semináře Optické komunikace 1984*, Praha, 1984, pp. 33-34.

[9] M. Pospíšilová, J. Veselý, "Měřící metody vláknové optiky," in *Sborník semináře Optické komunikace 1984*, Praha 1984, pp. 35-36.

[10] M. Sedlář, V. Matějec, "Fyzikálně chemický model přípravy vysokokřemičitých vláken dopovaných fluorem," in *Sborník konference Optické komunikace´ 88*, Praha, 1988, pp. 130-131.

[11] V. Matějec, A. Spáčilová, M. Pospíšilová, M. Hayer, J. Götz, "Příprava a vlastnosti různých typů jednovidových vláken," *in Sborník konference Optické komunikace´ 88*, Praha ,1988, pp. 132-136.

[12] V. Matějec, M. Sedlář, S. Poláková, " Příprava optických křemenných vláken dopovaných oxidy Nd a Er, " *in Sborník konference Optické komunikace´ 90*, Praha, 1990, pp. 73-77.

[13] V. Matejec, L. Sasek, J. Götz, G.A. Ivanov, N.A. Koreneva, V.V. Grigoryants, "New gas-phase etching method for preparations of plarization maintaining fibers," *in Proc. SPIE 1513 -Glasses for Optoelectronics*, 1991, pp. 174-179.

[14] J. Götz, Z. Choc, V. Matějec, M. Hayer, G. Kuncová, M. Pospíšilová, "Technologická příprava telekomunikačních vláken typu GI," *in Sborník konference Optické komunikace´ 88*, Praha 1988, pp.. 95-99.

[15] Z. Choc, O. Sysala, K. Matějovič, I. Kašík, M. Hayer, J. Zátorský, M. Pospíšilová, A. Spáčilová, J. Götz, "Technologie přípravy gradientních vláken pro telekomunikační systémy," *in Sborník konference Optické komunikace´ 90*, Peaha, 1990, pp. 68-72.

[16] I. Kašík, O. Sysala, J. Götz, "Dopování křemenných vláken netradičními dopanty," *Ceramics-Silikaty 36*, pp. 169-179, 1992.

[17] I. Kasik, V. Matejec, J.Kanka, P. Honzatko, "Properties and fabrication of ytterbium–erbium co-doped silica fibres for high-power fibre lasers," *Pure Appl. Opt. 7*, pp. 457–465, 1998.

[18] I. Kasik, P. Peterka, J. Mrazek, P. Honzatko, "Silica optical fibers doped with nanoparticles for fiber lasers and broadband sources," *Current Nanoscience 12*, pp. 277-290, 2016.

[19] V. Matejec, M. Chomat, M. Hayer, I. Kasik, D. Berkova, "Development of special optical fibers for evanescent-wave sensing," *Czech J. Phys. 49*, pp. 883-888, 1999.

[20] J. Skokankova, J. Mrazek, V. Matejec, M. Hayer, I. Kasik, M. Chomat, D. Berkova, A. Barau, M. Zaharescu, M. Raileanu, "Properties of xerogel layers for the detection of toluene in water," *Mater. Science Engineering* C26, pp. 208-213, 2006.

[21] P.J. Scully, L. Betancor, J. Bolyo, S. Dzyadevych, J.M. Guisan, R. Fernandez-Lafuente, N. Jaffrezic-Renault, G. Kuncova, V. Matejec, B. O'Kennedy, O. Podrazky, K. Rose, L. Sasek, J.S. Young, "Optical fibre biosensors using enzymatic transducers to monitor glucose," *Meas. Sci. Technology 18*, pp. 3177-3186, 2007.

[22] I. Kasik, J. Mrazek, T. Martan, M. Pospisilova, O. Podrazky, V. Matejec, V. Matejec, K. Hoyerova, M. Kaminek, "Fiber-optic pH detection in small volumes of biosamples," *Anal. Bioanalytical Chemistry 398*, pp. 1883-1889, 2010.

[23] V. Matejec, J. Mrazek, M. Hayer, O. Podrazky, J. Kanka,, I. Kasik, "Sensitivity of microstructure fibers to gaseous oxygen, " *Mater. Science Engineering C28*, pp. 876-881, 2008.

[24] V. Matejec, O. Podrazký, I. Kašík, M. Frank, M. Jelínek, V. Kubeček, "Comparison of characteristics of Bragg fibers with silica and air cores," *in Proc. SPIE 9450 –Photonics, Devices and Systems VI,*, 2015, paper 94500Y (8 pages) .

# On Measurement and Analysis of FSO Terminal Fixture Vibrations

Marek Novak, Petr Skryja and Peter Barcik

*Dept. of Radio Electronics, Brno University of Technology*
*Technicka 12, CZ-61600 Brno, Czech Republic,*
*Email: xnovak0m@stud.feec.vutbr.cz*

***Abstract*—The article presents a system whose task is to gather vibration data from Free Space Optical (FSO) communication terminal fixture. The purpose of gathered data is to analyze the response of the mechanical fixture to wind blasts. The paper provides a three-axis time evolution of vibration of the fixture measured by described system. After frequency analysis of this data a resonant frequency of the fixture was obtained and the dumping of the mechanical oscillations was measured. The obtained data from the measurement can be used to separate and compare the effects of vibrations and atmospheric turbulence on reliability and availability of the FSO link.**

***Index Terms*—Free Space Optics, Fixture, Vibration, Accelerometer, Mechanical Oscillations**

## I. Introduction

THE atmosphere and specifically the wind influences the FSO link performance. The FSO terminals are usually placed on the roof of the buildings or high pools which are places exposed to burst of high speed wind throughout the year. These wind gusts are responsible for vibration and deflection of terminal's fixtures. As a results the FSO link can be misaligned. This phenomenon sometimes cause misunderstanding the measured data. For example when measuring the angle of arrival or beam wandering of the optical wave due to atmospheric turbulence.

Vibration of the FSO terminals is very important in the context of fully photonic FSO systems. Fully photonic means that incoming optical beam is focused using a Fast Steering Mirror (FSM) into an optical fiber [1]. The fiber core diameter is in the order of tens of micrometers, therefore any vibration source or atmospheric turbulence deviate the beam and causes a signal loss [2]. In order to find the influence of wind on the parameters of the FSO link the attenuation of the link can be correlated with wind direction and speed [3].

Within the paper we build up the system for monitoring the FSO terminal's vibration due to wind or another mechanical distractions. The gathered vibration data can be compared with data from meteostation which is placed next to the monitored terminal. The analysis of present vibrations helps to improve the Acquisition, Tracking and Pointing (APT) algorithm and to reduce the impact of these effects. An accelerometer method for vibration measurement is used and compared with an optical method.

## II. Methodology

In order to monitoring the vibration on FSO terminal we set up the measuring device based on raspberry pi embedded computer. To measure vibration, accelerometer ADXL345 was used. It is ultralow power, 3-axis accelerometer with resolution of 10-bit (maximum 13-bit) which allows measurement at up to ±16g. Because the vibration of the fixture is very low, the accelerometer is set to resolution ±2 g. A sensitivity for this range is typically 256 LSB/g. Noise for the axis is up to 1.1 LSBrms for selected range. The accelerometer is connected by I2C peripheral to Raspberry Pi microcomputer which is responsible for reading data from the sensor. Data transfer of the I2C communication is set to 400 kHz and data are read with frequency of 80 Hz. The data are then sent by WiFi or Ethernet connection to a server, where they are stored for later analysis. Fig. 1 shows the diagram of the measuring system.

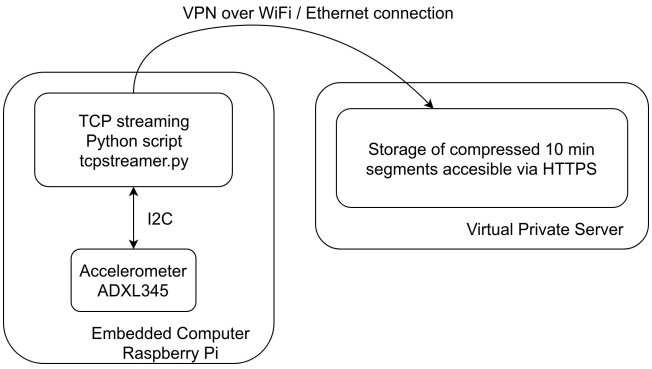


Fig. 1. Block diagram of logging vibration system.

The measuring device was firmly attached to the monitored terminal. The accelerometer can measure acceleration in three axis depicted in Fig.3.

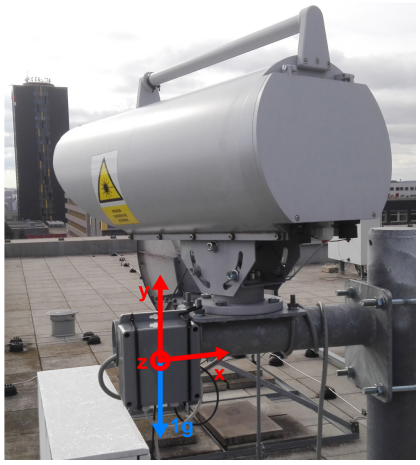


Fig. 2. Prototype of device for vibration measurement installed on FSO fixture.

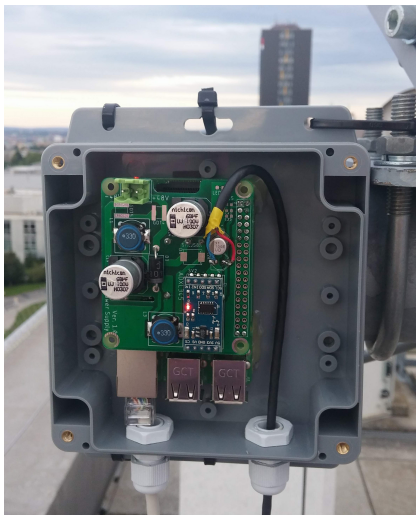

Fig. 3. Prototype of device for vibration measurement.

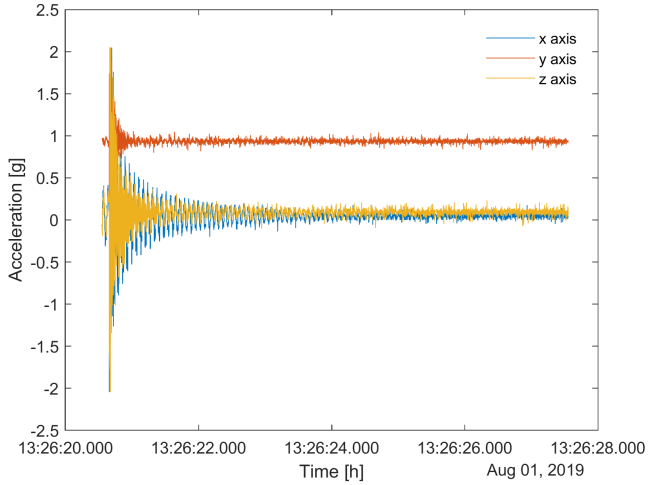


Fig. 4. Oscillation of artificial created vibration in time domain.

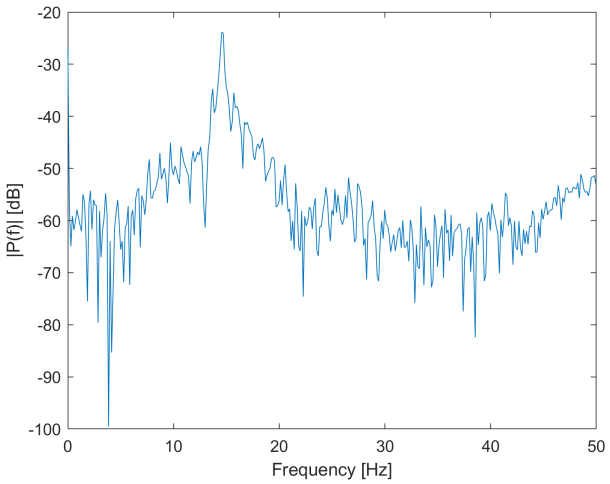


Fig. 5. Oscillation of artificial created vibration in frequency domain (x axis).

## III. Results

Firstly we carried out measurement for artificially created vibrations. The resulting vibration data are then shown in time domain in Fig. 4 and the frequency analysis (spectrum in Fig. 5) helped to measure the resonant frequency of the vibrating fixture. According to Fig. 5 it is 14.6 Hz. From the time domain graph, it can be seen that there is a dumping effect in the signal, which if known, along with the resonant frequency, allows to predict the movement of the whole fixture after an air gust.

In order to find out response of the terminal to wind gusts we carried out long term measurement. The recorded data was gathered and then compared with data from meteostation. We picked up interesting data from 30th of September 2019. The Fig. 6 depicts accelerations in axis x, y and z. It is clear that amplitude of vibrations induced by wind is very low in comparison with artificially excited vibrations. The vibrations are strongest in y axis. According to frequency spectrum depicted in Fig. 7, the vibrations have frequency of 10 Hz. For comparing the vibration data with wind speed and wind direction we plotted only data from y axis (Fig.8). Because of low vibration amplitude and low sampling rate of the meteostation it is hard to detect the wind gusts responsible for fixture vibration. The meteostation was able to record data every 15 seconds. We found out that there is a delay 4 minutes between data from meteostation and data from vibration measurement system caused by averaging of the data in meteostation.

The minima and maxima in Fig. 6 reach respectively 0.90 g and 1.15 g acceleration with a mean value of 1.0 g. These values of fixture acceleration (corresponding to mechanical vibration) were obtained for wind speeds reaching up to 30 km/h, which corresponds to level 5 of Beaufort wind force scale. This

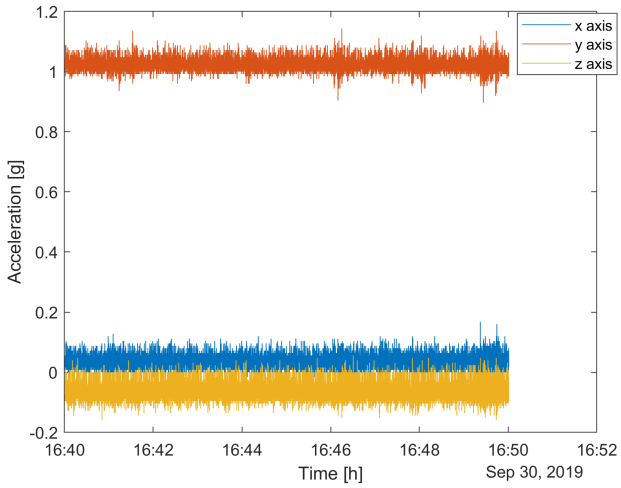


Fig. 6. Acceleration of the fixture in x, y and z axes

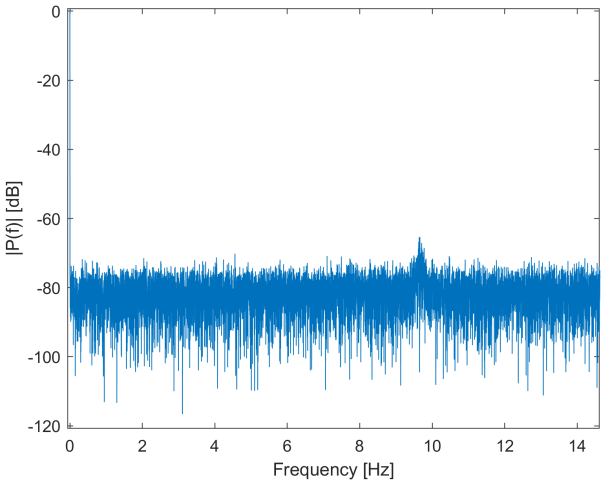


Fig. 7. Spectrum of measured acceleration data (y axis).

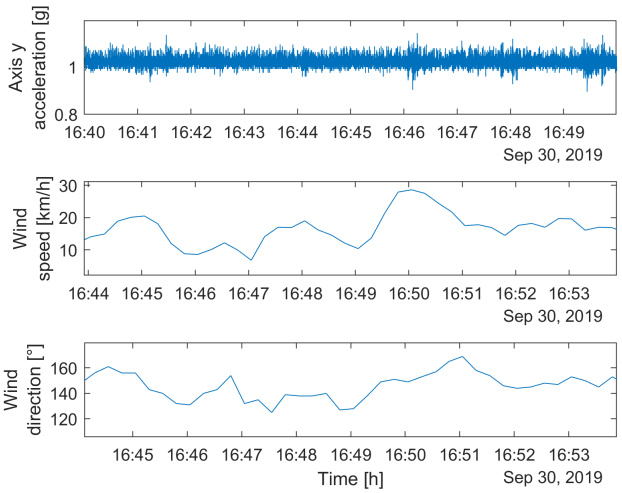


Fig. 8. Comparison of acceleration in x axis with the wind speed and direction

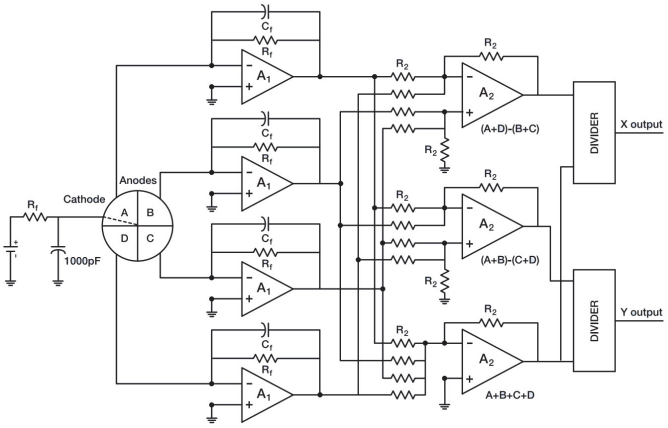


Fig. 9. Circuit for position detection using PSD [5]

is rather above the average for the urban area in the city of Brno, where the measurements were accomplished, according to the average wind speed graph available in [4]. Therefore, for increasing the applicability of vibration measurement to normal weather conditions, it is necessary to increase the sensitivity of used sensor. The future research will consist of evaluation the optical method based on segmented PSD (Planar Diffused Photodiodes).

A segmented PSD consists of four segments with common cathode, which is in the center of the active area of the photodiode array. Fig. 9 shows a typical circuit beam position detection, which can be used for vibration measurements, if the laser beam transmitter is positioned on a fixed non-vibrating fixture (under the FSO terminal). As the PSD receiver side vibrates, the beam spot moves which is tracked by the X and Y signals (Eq. 1, 2).

$$X = \frac{(A+D)-(B+C)}{A+B+C+D} \tag{1}$$

$$Y = \frac{(A+B)-(C+D)}{A+B+C+D} \tag{2}$$

## IV. Conclusion

Within the paper, the system for measuring vibration of the FSO fixture was described. The experimental data for artificially excited fixture and wind gust excited fixture were reported. The frequency response of the FSO fixture was measured for both cases. Based on this known response, a mathematical model will be created allowing making a short-time prediction of FSO terminal deviation, which will be used in the APT algorithm. The next research will be focused on improvement of the measurement system's sensitivity.

## ACKNOWLEDGMENT

This work has been supported by projects VI20192022173 and FEKT-S-17-4707.

## REFERENCES

[1] P. Barcik, O. Wilfert, A. Dobesch, Z. Kolka, L. Hudcova, M. Novak, and E. Leitgeb, "Experimental measurement of the atmospheric turbulence effects and their influence on performance of fully photonic wireless communication receiver," *Physical Communication*, vol. 31, pp. 212 – 217, 2018.

[2] M. Matsumoto, K. Osawa, S. Hotta, and K. Wakamori, "Innovative tracking system for next generation fso systems under massive earthquakes," in *2015 International Conference on Optical Network Design and Modeling (ONDM)*, May 2015, pp. 233–238.

[3] V. Brazda, O. Fiser, Z. Chladova, J. Poliak, and V. Schejbal, "On wind influence on fso link attenuation," in *2013 7th European Conference on Antennas and Propagation (EuCAP)*, April 2013, pp. 966–968.

[4] D. Hanslian, J. Hosek, Z. Chladova, and L. Pop. (2013) Vetrne podminky v ceske republice ve vysce 10 m nad povrchem i. [Online]. Available: https://oze.tzb-info.cz/vetrna-energie/9770-vetrne-podminky-v-ceske-republice-ve-vysce-10-m-nad-povrchem-i

[5] *Photodiode Characteristics and Applications*, UDT Sensors, Inc., 2002.

# Inner-cladding Shaping Based Pump Absorption Enhancement

Ali A. Jasim, Ivan Kašík, Pavel Honzátko

*Institute of Photonics and Electronics of the Czech Academy of Sciences, Chaberská 57, 182 51 Prague, Czech Republic.*

***Abstract*— Optical fibers for use in high-power fiber lasers and amplifiers have designed much different from standard telecommunication optical fibers. Although the conventional single-mode fibers can guarantee single-mode propagation in the core, they suffer from low coupling efficiency to multimode pump sources and pump absorption saturation. Therefore, the active fibers designed for the use in high-power fiber lasers should have a double-clad structure with a high numerical aperture of the inner-cladding in order to provide good coupling with high-power multimode pump laser diodes. Besides, the inner-cladding should be designed with a noncircular structure to further scramble pumping modes, which in turn increases the spatial overlap with the signal in the core and improves pumping absorption efficiency. However, there still exists a pressing question of what is the best cross-section shape of the inner-cladding for efficient pump absorption and what method should be used for the fabrication of such shaped fibers. In this work, we present some simulation results based on pump absorption enhancement in various complex shapes of double-clad fibers that only can be fabricated using the $CO_2$ laser-based optical fiber preform shaping. The simulation results show better absorption achieved in the fibers were inner-cladding has U-shape-grooves compared to the V-shape grooves.**

***Index Terms*—Double-clad fibers, $CO_2$ laser, Optical fiber preform, pump absorption enhancement.**

## I. INTRODUCTION

Fiber lasers proved to have many advantages over the solid-state glass lasers owing to their features of compact volume, high beam quality, high laser efficiency, and low noise floor [1]. This is due to the remarkable development of designing active fiber based on double-clad (DC) structure, where it has enhanced the pumping technology with high power multimode laser diodes and thus kilowatt lasers are now available with more than 80% efficiency [2-3]. DC fiber features two different numerical aperture (NA) of the fiber core and of the inner cladding structure. The large NA of the inner-cladding of the DC fiber allows efficient coupling of the multimode pump, while the small NA of the fiber core retains the single-mode propagation and amplification of the signal. Besides the optimal concentrations of the dopants in the fiber core, the shape of the inner-cladding is key to power scaling in fiber lasers. The noncircular symmetry of the inner-cladding prevents the development of skew modes that never interact with the doped fiber core. The optical fiber preforms had to be shaped prior to fiber drawing. Based on the recently reported rigorous theoretical description of the mode mixing in double-clad fibers, promising concepts of new fiber geometries and layouts for tailoring the pump absorption have been investigated [4-7]. However, there is still an existing pressing question of what is the best inner-clad cross-section shape for efficient absorption. A new technique of thermally shaping optical fiber preform based on $CO_2$ laser is now available [8, 9] along with the conventional mechanical-based grinding. Such a technique enables shaping optical fiber preforms to have a cladding structure with concave and convex surfaces that not limited to sharp and flat shapes like the shapes obtained based on the conventional shaping technique.

In this work, we will present some simulation results based on pump absorption enhancement in various complex shapes of inner-cladding of DC fibers that are only achievable by shaping optical fiber preform with a $CO_2$ laser. The simulation results show that the pump absorption can significantly be enhanced in the fibers were their inner-cladding has U-shape-grooves compared to the V-shape grooves.

## II. OPTICAL FIBER PREFORM SHAPING BASED ON CO2 LASER

It's a recent innovative technique that enables shaping optical fiber preform thermally using a carbon dioxide CO2 laser (10.6 μm). This technique profits from a high absorption of the silica glass at wavelengths around 10.6 μm. Figure 1 shows a developed homemade $CO_2$ laser-shaping machine employed for shaping. The machine consists of two 3D-translation stages holding the optical preform from both sides and placed below the $CO_2$ beam laser. The machine was designed to provide a high-quality shaping process to various preform shapes. One of the advantages of this technique is that fiber preform can be processed to complex shapes. By control of beam radius and ellipticity, grooves of V-shape and U-shape can be made on the optical fiber preform surface.

The process of shaping optical preforms consists of a few steps of exposing laser onto the preforms. First, we evaporate the silica out of the preform surface by applying high power of $CO_2$ laser with a slow speed of expositions. In this step, the preform surface gets rough with some dry silica soots left on it. The soots can be removed and surface smoothened by applying lower laser power with a fast speed of expositions [9]. The time spent for shaping under this technique depends on the number of shaping steps as well as on the applied laser power. Figure 2 shows a real image of a longitudinal section of shaped optical fiber preform. Once the process of shaping preforms finished, the preform can be drawn to DC fibers. Figure 3 illustrates two cross-sections achievable with laser beams of different parameters.

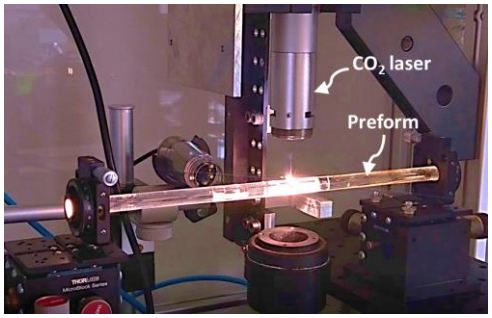


Fig. 1. Real image of thermally shaping optical fiber preforms technique with CO2 Laser.

Fig. 2. Real image of thermally shaping optical fiber preform based $CO_2$ laser.

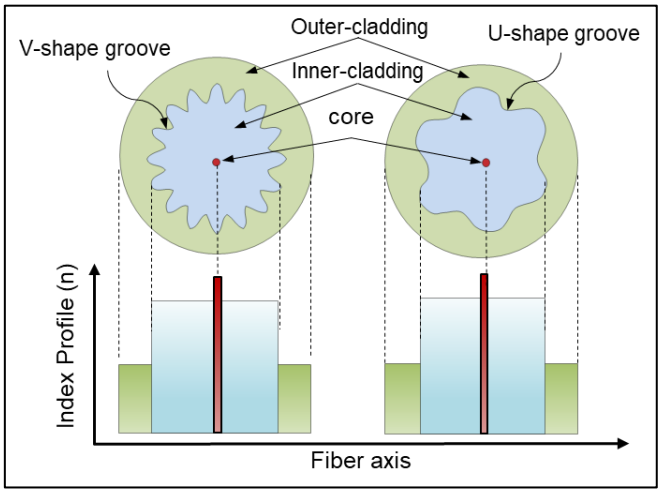


Fig. 3. Illustration of two kinds of shaping DC fibers based U-shape grooves and V-shape grooves with respect to the employed ZnSe lenses.

## III. Simulation Results

Simulations were performed by the scalar beam-propagation method in RSoft. We simulated a fiber bent with an effective radius of 15 cm. The direction of bending is changed to the opposite after every 30 cm of propagation. The fibers used in the simulations were 1.2-meter-long and have a geometry of 13/105/125 µm (core/inner-cladding/outer-cladding diameter) and NA 0.12/0.46 (core/clad), as shown in figure 4. Distribution of the pump power along the fiber was calculated for different inner-cladding shapes and compared with a straight and bent fiber of circular inner-cladding. Figure 5 (a) and (b) compares the distribution of the pumping power along the circular straight and bent fiber, respectively. It can be seen that less than 34% of the pump power is absorbed in the straight circular fiber (Fig. 5(a)) while in the circular fiber with alternating bending it is more than 62%. This because the alternating bending improves effectively scrambles pumping modes, which in turn increases their spatial overlap with a fiber core and improves the pump absorption efficiency. In another word, the bending improves greatly the absorption in the fiber core.

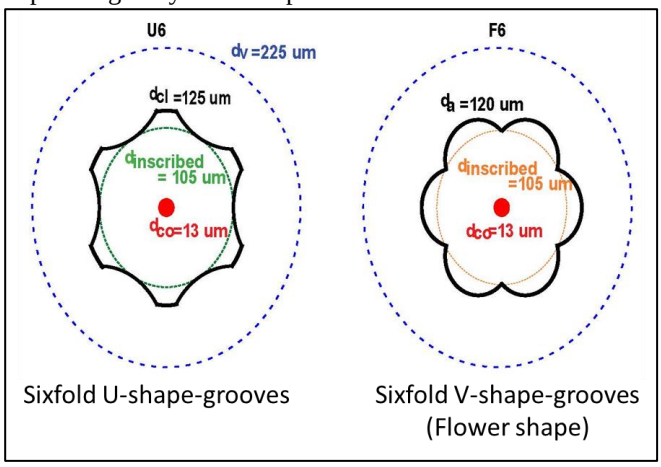


Fig. 4. Illustrated cross-section of sixfold shaped DC fibers used in the Rsoft simulations.

This pump absorption can be further increased by shaping the inner cladding as shown in figure 6. Fibers with flower-shaped inner cladding with 6 and 8 leaves absorb 72% and 75% of pump power, respectively.

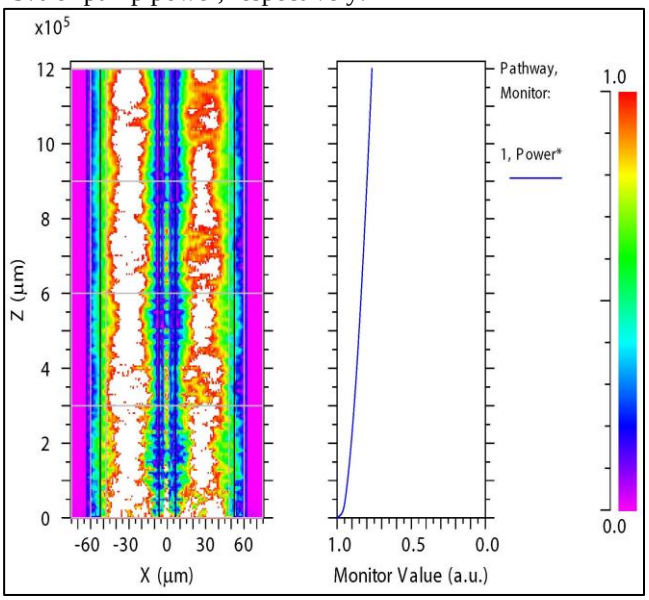


(a)

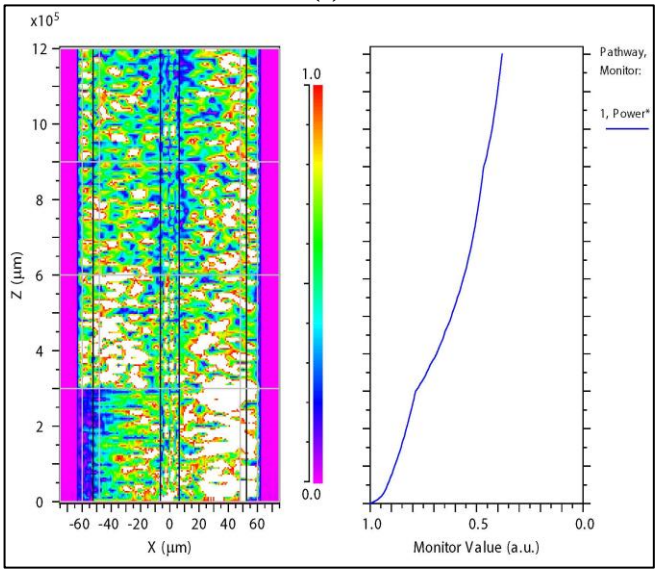

(b)

Fig. 5. The calculated pump absorption in the circular unshaped fiber. (a) under a case of straight packaging, (b) under the case of bend packaging.

Even better results can be achieved with U-shape-grooves made into the inner cladding (Figs. 6, 7). Here the pump absorption can be as high as 82.9% for 6 grooves and slightly worse, 77.8% for 8 grooves. This is probably because 8 grooves in the inner-cladding may make the shape of the fiber closer to the circular shape and thus provide less absorptions.

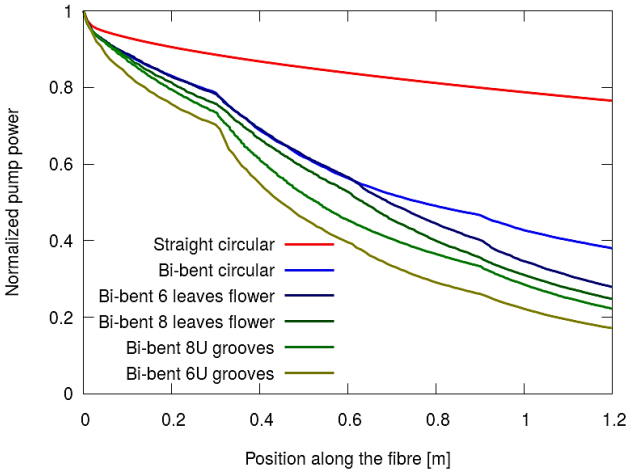


Fig. 6. Pump absorption along a straight and bent circular fiber as well as different bent shaped fibers.

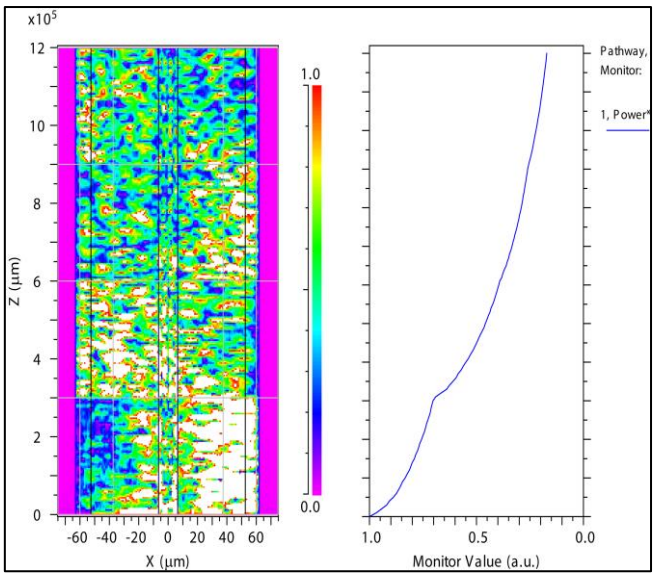


Fig. 7. The calculated pump absorption in the 1.2-m-length fiber has inner-cladding of sixfold U-shape-grooves.

## IV. Conclusion

Pump absorption of the fiber laser can be enhanced by breaking the circular symmetry of the inner-cladding of the DC fiber. Using a $CO_2$ laser as a new innovative technique of optical fiber preforms processing, various complex shapes can be obtained, thus providing more flexibility in pump modes scrambling. For the particular fiber used in the simulations, the highest pump absorption is achieved with the inner-clad with U-grooves and sixfold symmetry.

## References

[1] Ter-Mikirtychev, Valerii Vartan. *Fundamentals of fiber lasers and fiber amplifiers*. Springer, 2014.

[2] M. N. Zervas and C. A. Codemard, "High Power Fiber Lasers: A Review," *IEEE J. Sel. Top. Quantum Electron*., Vol. 20, no.5, pp. 219-241, 2014.

[3] D. J. Richardson, J. Nilsson, and W. A. Clarkson, "High power fiber lasers: Current status and future perspectives," *J. Opt. Soc. Amer. B*, vol. 27, pp. B63–B92, 2010.

[4] C. A. Codemard, A. Malinowski, and M. N. Zervas, "Numerical optimisation of pump absorption in doped double-clad fiber with transverse and longitudinal perturbation". In Fiber Lasers XIV: Technology and Systems, *Int. Soc. Opt. Photonics*, Vol. 10083, p. 1008315, 2017.

[5] A. A. Jasim, J. Aubrecht, P. Peterka, M. Kamrádek, O. Podrazký, F. Todorov, I. Kašík and P. Honzátko, "Efficient Pump Absorption in Twisted Double Clad Thulium-Doped Fibers Drawn of CO2 Laser Shaped Preform," In Proc. *CLEO-Europe and EQEC*, München, CJ-p-8, 2019.

[6] P. Koska, P. Peterka, J. Aubrecht, O. Podrazky, F. Todorov, M. Becker, Y. Baravets, P. Honzatko, and I. Kasik, "Enhanced pump absorption efficiency in coiled and twisted double-clad thulium-doped fibers," *Opt. Express*, vol. 24, no. 1, pp. 102-107, 2016.

[7] P. Koska, P. Peterka, and V. Doya, "Numerical modeling of pump absorption in coiled and twisted double-clad fibers," *IEEE J. Sel. Top. Quantum Electron*., vol. 22, no. 2, pp. 55-62, 2016.

[8] P. C. Shardlow, R. Standish, J. Sahu, and W. A. Clarkson, "Cladding Shaping of Optical Fibre Preforms via CO2 Laser Machining," in European Conference on Lasers and Electro-Optics, *Opt. Soc. Am*., CJ-P-29, 2015.

[9] A. A. Jasim, O. Podrazký, P. Peterka, F. Todorov, and P. Honzátko, "Experimental investigation and characterization of fabrication shaped clad optical fiber by thermally polishing optical fiber preforms with CO2 laser," in Micro-structured and Specialty Optical Fibres VI, *Int. Soc. Opt. Photonics*, vol. 11029, p. 1102909, 2019.

# Differential gain comparison of optical planar amplifier on silica glasses doped with Bi-Ge and Er, Yb ions

Jiří Šmejcký, Vítězslav Jeřábek

*Faculty of Electrical Engineering, Technical University in Prague*

*Abstract* –The paper presents the calculation of the planar optical amplifier gain and the optimal length of the active optical amplifier waveguide doped with Bi-Ge radiation complexes compared to an optical amplifier with active doping with ions Er, Yb. At present are using optical amplifiers for the high-capacity optical communication systems in the narrow spectral region of 1530–1560 nm, determined by the gain bandwidth of erbium-doped fiber amplifiers (EDFA) or erbium-doped optical planar amplifiers (EDPA) realized as active planar waveguides in the optical integrated circuits technique. However, it is possible increase wavelength region up to 1610 nm, where optical losses of telecommunication fibers are less than 0.3 dB per km, if appropriate amplifiers are available. In this regard, the development of novel optical amplifiers operating in this spectral region have of great importance. The paper summarizes the results measurement and calculation of the transmission characteristics of the amplification of the new active silica glass structures and possibilities novel optical amplifiers for extension of the bandwidth from 1530 to 1610 nm doped by bismuth- erbium ions.

## 1. INTRODUCTION

In optical telecommunication systems, optical amplifiers are one of the essential parts of the optical transmission tracts containing silicon fiber waveguides. The main part of optical amplifiers is an optically active fiber waveguide. The information capacity of an optical fiber transmission path is determined by the width of a spectrum of optical amplifiers that use the quantum principle of stimulated radiation and are extensively wave selective. Their selectivity depends on the type of activator that is used to amplify the passing radiation. In order to expand the transmission capacity of the connection, it is necessary to extend the bandwidth of the optical amplifiers. This is possible by using two or more activators in the optical fiber optic amplifier waveguide. In the last few years, several works have been published on broadband fiber active waveguides for optical amplifiers in telecommunication bands. These waveguides contain erbium and bismuth ions [1], [2] for medium wavelength telecommunication bands at 1340, 1430 and 1700 nm. Broadband optical transmission systems are currently being implemented with parallel optic amplifiers. However, the use of several separate optical amplifiers for broadband telecommunication systems is not optimal, both economically and technically. A more preferable solution would be to use a fiber or planar amplifier with a high bandwidth amplifier, for example for S + C + L (1460 - 1615 nm) or C + L + U (1530 - 1675 nm). Many attempts have been made to achieve optical amplification using erbium and bismuth codoped optical waveguides for broadband near-IR (NIR) band systems. Unfortunately, until now, the continuous spectral range of these materials has not been demonstrated in the desired wavelength range.

The problem consists in that the luminescence spectrum typical of bismuth and erbium-doped active waveguides has a slight overlap, especially for shorter wavelengths. For this reason, it is not possible to implement a broadband amplifier with a balanced amplification in the band S + C + L (1460 - 1615 nm).

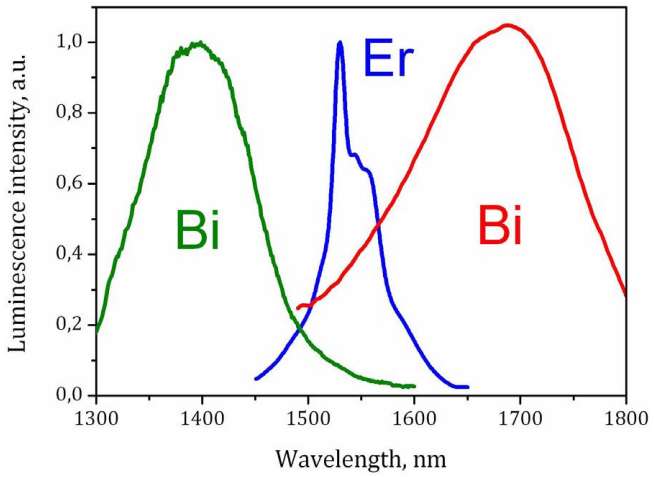


Fig. 1. Typical luminescence spectrum of fiber doped Bi and Er [3].

Somewhat more promising seems to be the use of the band C + L + U (1530-1675 nm), where the overlap of the luminescence spectrum of erbium and bismuth is stronger, see Fig. 1.

### 2.1 Introduction to broadband optical waveguide issues

At present, optical amplifiers for high-capacity optical communication systems in the narrow spectral range of 1530-1560 nm are used, which are determined by the erbium-doped fiber amplification bandwidth (EDFA) or optical planar amplifiers doped with erbium (EDPA) as active planar waveguides in the optical integrated circuits. However, when suitable amplifiers are available, it is possible to increase the range of wavelengths up to 1610 nm, where the optical loss of telecommunication fibers is less than 0.3 dB / km. In this respect, the development of new optical amplifiers operating in this spectral range is of great importance.

In the study of [2], the output optical power of bismuth/ erbium doped optical fiber (BEDF) was studied in double pumping at 830 nm and 980 nm., Based on these experiments, the possible energy transitions of the BEDF were proposed. The measurement results demonstrate the benefits of pumping BEDF at 830 nm versus 980 nm in terms of

absorption, pumping efficiency, excited state absorption and amplification. Since the first demonstration of broadband emission in glass doped with bismuth [4], attention has increasingly been paid to active Bismuth-doped waveguides for their potential use as active media for broadband amplifiers and super-luminescent sources in the spectral range of 1150-1800 nm. Bismuth-doped waveguides have a wavelength range of 1100-1600 nm. Their fluorescence strongly depends on the wavelength of the pumping radiation because they contain several active centers (bismut active centers - BACs) with different excitation and emission spectra. This makes it possible to adjust the excitation and emission wavelengths by a type of modifier such as Al, Si, Ge or P. This feature allows you to fine-tune the power of the active bismuth-doped fibres (BDF) by selecting the wavelength of the pumping source. It also shows that BACs are very complicated in nature. It was also shown [2] that the profile and bandwidth can also be selected and set by the appropriate choice of the source(s) wavelength. Due to the existence of more active bands in the BDEF waveguide, it is advantageous to carry out simultaneous pumping at multiple wavelengths. A comparison of the BEDF power output at the wavelength of 830 nm was made 980 nm. At that, waveguide attenuation, luminescence properties and on-off gain were measured. By analyzing absorption, amplification, and ESA at 830nm and 980nm, two different energy conversion processes were designed and an attempt was made to explain the broadband emission in the BEDF.

### 2.2 Measurement of the fiber waveguide

The research study [1] describes the production of a BEDF waveguide on which the measurement was done, Fig. 2.

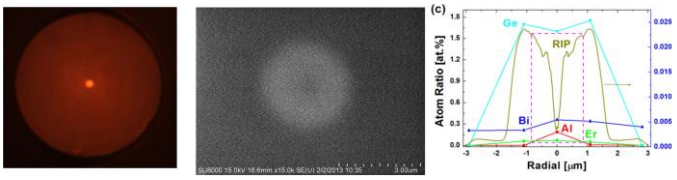


Fig. 2. (a) Cross-sectional image of BEDF; b) image of the BEDF core region SEM; c) BEDF composite radial element and refractive index (RIP) profile (the dashed-line rectangle is the area of impact) [1].

In Fig.2a,b is a cross section of the waveguide obtained with a scanning electron microscope. It can be observed that the waveguide can be considered rotationally symmetrical. Fig. 2c is a profile of composite radial element with a plurality of additional dopants (germanium, phosphorus, aluminum, etc.) and wavelength core refractive index waveform (RIP).

### 2.3 Absorption spectral characteristics

On this active optical waveguide, the attenuation was first measured (Fig. 3). The graph of the spectral damping characteristics shows the spikes at points around 500 nm (A), 730 nm (B), 820 nm (C), 950 nm (D), 1000 nm (F) and 1400nm (F), with peaks of 550 and 1530 nm being attributed to $Er^{3+}$. Together BAC-Ge, $Bi^{2+}$ and BAC-Si are responsible for the attenuation bands around points A, B, C. Gaussian selection (filtering) distinguished three attenuation zones in the range of 920 to 1100 nm. These are attenuation peaks around wavelengths ~ 950, ~ 980 and ~ 1020 nm which are attributed to the absorption of BAC-Ge, $Er^{3+}$ and BAC-Al. In addition, there are also three attenuation bands between 1100 and 1480 nm, which are attenuations at ~ 1350, ~ 1380 and ~ 1410 nm for which BAC-P, OH and BAC-Si are responsible. Spectral Attenuation Characteristics shows the possibility of pumping BEDF at 730 nm (BAC-Ge), 830 nm (BAC-Si) and 980 nm (BAC-Al and $Er^{3+}$). Additionally, the attenuation coefficient at 730 nm (21,5 dB/m) and 830nm (30.9 dB/m) is approximately three and four times larger than at 980 nm (7.7 dB/m). Absorption effective cross-section at 830 nm is greater than at 980 nm.

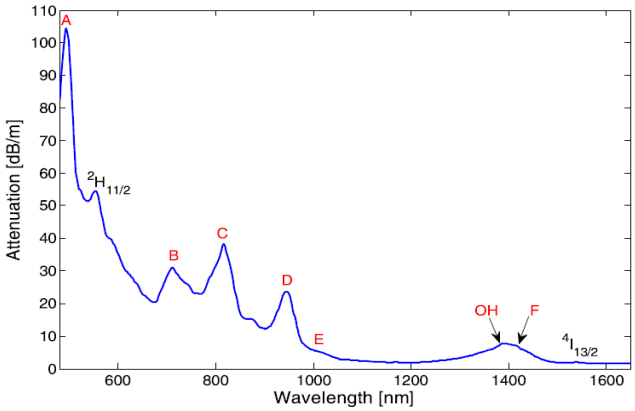


Fig. 3 BEDF Attenuation Spectrum [1].

### 2.4 Emission spectral characteristics BEFD

The emission spectrum of BEDF excited at 830nm and 405 nm was measured. The normalized emission spectrum is shown in Fig. 4

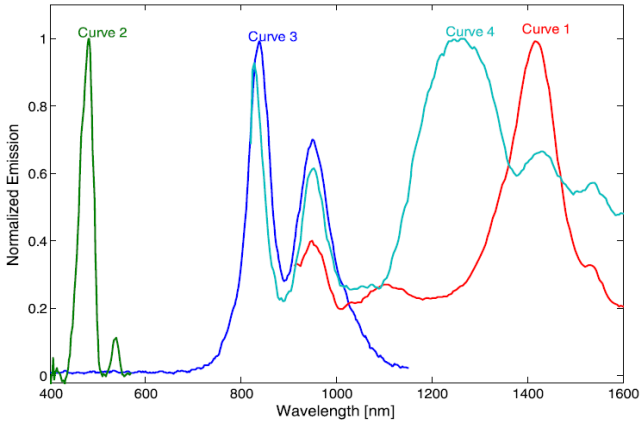


Fig. 4. Normalized emission spectra BEDF excited at 830 nm (curve 1 and curve 2) and 405 nm (curve 3 and curve 4) [1].

From the normalized emission characteristics, the existence of the six NIR emission bands (curves 1,3 and 4) occurring around ~ 830, 950, 1100, 1260, 1410 and 1530 nm where the first five bands belong to the BAC emission, 1530 nm corresponds to the electron transitions of the erbium ($^4I_{13/2}$ => $^4I_{15/2}$). The emission bands at 830, 1410, 950, 1110 and 1260 nm correspond to BAC-Si, BAC-Ge, BAC-Al and BAC-P. In addition to NIR emissions, two UP-conversions in the bands 480 and 540 nm (curve 2) are identifiable. In addition, the NIR lifetime that is measured at wavelengths 950, 1110, 1260 and 1410 nm is approximately 110, 590, 150 and 450 μs.

Measuring the life of metastable states corresponds well with the emission spectrum analysis and confirmed the existence of four BACs: BAC-Ge, BAC-Al, BAC-P and BAC-Si. The results of the measurements of the metastasis statuses indicate

that the most stable is the metastable state of BAC-Ge (590 μs).
Comparison of emission spectral characteristics for single or double pumping. The measurements were made in the arrangement shown in Fig. 5. The measured characteristics are shown in Fig. 6.


Fig. 5. Experimental setup for the backward emission measurement with 830 nm or 980 nm, pumps. [1]

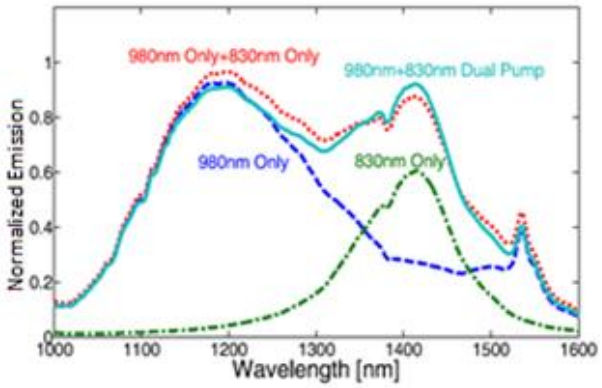


Fig. 6. Experimental measurements of emissions while using 830 nm or 980 nm pumps, alternatively and concurently [1].

In the experimental system, the Optical Spectrum Analyzer (OSA) was used to record backward emission spectra of a 50 cm long BEDF. Laser diodes 830 nm and 980 nm were connected via WDM 800/1000 nm multiplexer to the measured waveguide. The power meter was connected to the output of the waveguide to monitor the residual pumping power for luminescence analysis. From the graph in Fig. 6 we can clearly see one emission band at 1410 nm (BAC-Ge) when pumping only at 830 nm. When pumping only at 980 nm, there are two emission zones, namely 1190 for BAC-Al and BAC- P and 1536 nm for $Er^{3+}$. By way of comparison, Fig. 6 shows the dependence of the emission on pumping power for pumping wavelengths of 830 nm and 980 nm . It is clear that the emission at 830 nm pumping is growing much faster than when pumping at 980nm.
More detailed information and design of BEDF energy transfer diagram at pumping 980 nm and 830 nm is given in the work [6].

### 2.5 Optical amplifier for C + L + U telecommunication bands

The results of the experimental measurement by bismuth are remarkable. However, for the third optical quench window of quartz waveguides NIR, the band between 1500nm and 1700nm is needed. In the study of [3] a fiber amplifier for C + L + U telecommunication area with continuous amplification in the band 1530-1675 nm (and more) is described. In this case, germanosilicate fibers are co-doped with various contents of bismuth and erbium that have been produced by the modified chemical vapor deposition method (MCVD). It should be noted that the BAC parameters are strongly dependent on the manufacturing parameters. Therefore, the production of an active optical waveguide with a corresponding Bi/Er ratio is one of the key issues. It is also known that the optical properties of the activated bismuth doped waveguide depend on the chemical composition of the glass from which they are made. Fig. 7 shows an absorbent spectrum of fibers with different Bi/Er ratios.

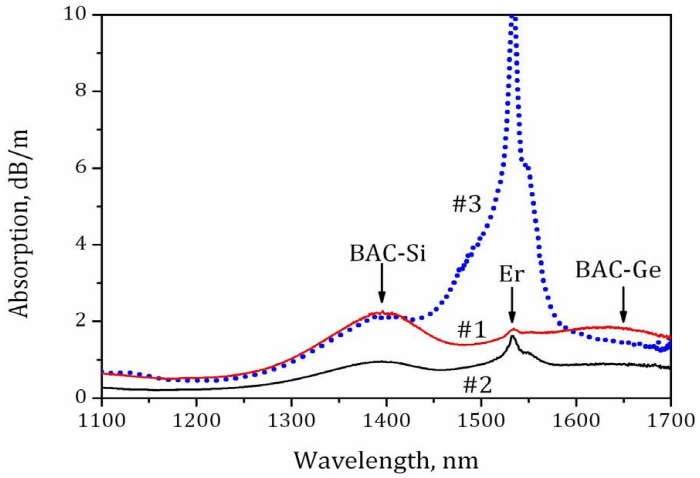


Fig.7. Absorption spectra of the various Bi/Er-codoped germano-silicate fibers. [3]

The graph shows two different absorption peaks at 1650 and 1400 nm, which belong to BAC-Ge and BAC-Si.
The absorption band with a peak at 1535 nm is assigned to $Er^{3+}$ ions. It can be seen that the BAC-Ge and Er bands overlap significantly. This fact is also schematically shown in Fig. 11, where the energy levels of $Er^{3+}$ + and BAC-Ge overlap. Therefore, for the excitation of both active centers, it is possible to use only one source of pumping radiation, in this case at a wavelength of 1460 nm. This is an indisputable advantage over the use of two pumping sources. In this case, when using only one source of pumping radiation at 1460 nm, a continuous gain in the range 1530-1675 nm was achieved Fig. 8.

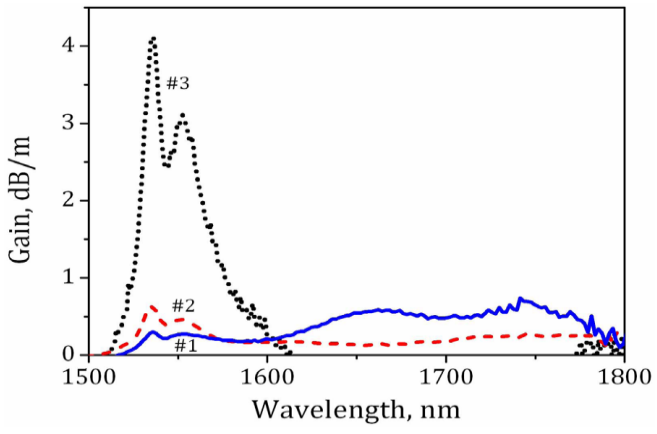


Fig. 8**.** Net gain spectra of the investigated fibers Bi/Er at pumping 1460 nm [3].

### 3.1 Theoretical analysis of the optical active waveguide

The theoretical analysis is based on a mathematical model that describes approximately the behavior of the optical active structures (waveguides) and allows to predict theoretically the quantum behavior of the structures and perform some optimizations on technological level. The behavior of the optical active structures is influenced by a number of factors, both the actual composition of the active material and its geometric configuration, the choice of pumping power, the active length of the waveguide.
Finding optimal concentrations of activators and precursors is one of the pivotal challenges in the development of optically active structures. At higher concentrations of activators, luminescence is extinguished by clustering of the activator atoms, energy migration or cross-relaxation. The Judd-Ofelt theory is used to assess the influence of matrix atoms on the active ions (activators). However, this optimization is not the subject of this work.
In this work, a mathematical model will be described which allows for the optimization of the length of the active structure and the choice of the pumping power on the basis of solutions of so-called rate equations and equation describing the propagation of the optical signal in the active optical waveguide.

### 3.2 Mathematical model of optical active waveguide

The calculation of the amplification of the optical active waveguide essentially resides in the solution of the system of differential equations describing the occupation of atomic levels (the so-called rate equations) and in the solution of propagation of light by the propagation equation. Differential velocity equations are derived from three basic phenomena describing the probability of the transition of the quantum system: spontaneous emission, stimulated emission and absorption (A. Einstein). The energy gradients in the erbium-ytterbium complex are described by absorption and emission effective cross-sections. For insulated non-degraded atoms, the following applies: $\sigma_e(\nu) = \sigma_a(\nu) = \sigma(\nu)$. In the real system, however, the energy levels are always degenerated and therefore the absorption and emission spectral waveforms differ : $(\sigma_e(\nu) \neq \sigma_a(\nu))$.

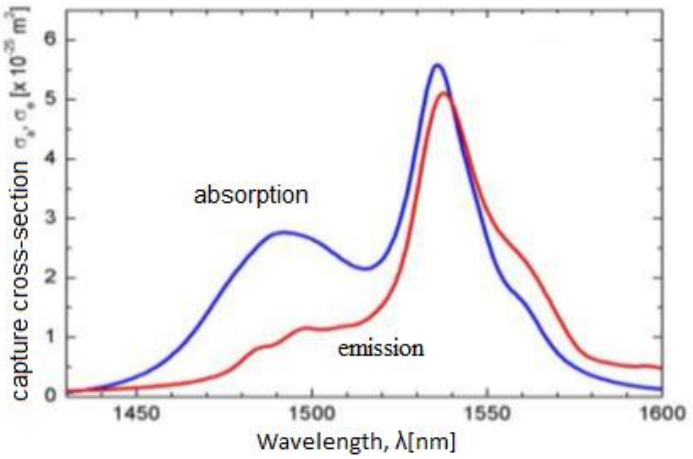


Fig. 9. Absorption and emission spectrum of the waveguide $Er^{3+}$ [5]

### 3.3 Rate equations for three-level system for Er and Yb

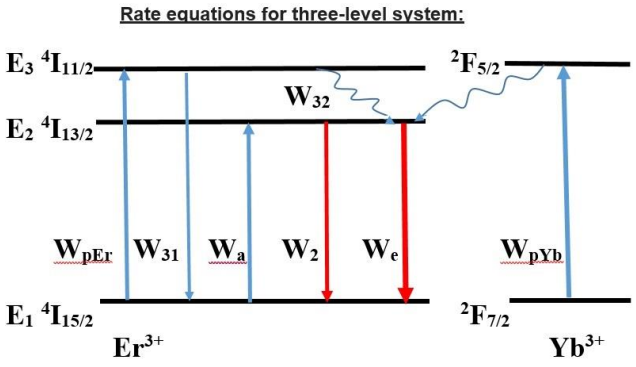


Fig. 10. The Erbium-Ytterbium complex can roughly be described as a three-level quantum system.

The Erbium-ytterbium complex can roughly be described as a three-level quantum system using rate equations in the form

$$\frac{dN_3}{dt} = -W_{32}N_3 - W_{31}N_3 + W_{pEr}N_1 \quad (1)$$

$$\frac{dN_2}{dt} = W_{32}N_3 - W_2N_2 - W_eN_2 + W_aN_1 + W_pN_1 \quad (2)$$

$$N_{tot}^{Er+Yb} = N_1 + N_2 + N_3 \quad (3)$$

where $N_1$ electron concentration on energy level $E_1$, $N_2$ electron concentration on energy level $E_2$, $N_3$ electron concentration on energy level $E_3$ and $W_{32}$ is the rate coefficient of non-radiation transition from $E_3$ to $E_2$, $W_{31}$ is the rate coefficient of non-radiation transition from $E_3$ to $E_1$, $W_2 = 1/\tau_2$ is spontaneous emission.

$W_p = \frac{I_p}{h\nu_p}(\sigma_{pEr} + \sigma_{pYb}) = W_{pEr} + W_{pYb} = \frac{I_p}{h\nu_p}\sigma_p$ is (4)

the rate coefficient pumped,

$W_a = \frac{I_s}{h\nu_\lambda}\sigma_{aEr}$ is the rate coefficient of stimulated (5)

absorption,

$W_e = \frac{I_s}{h\nu_\lambda}\sigma_{eEr}$ is the rate coefficient of stimulated (6)

emission.

In a three-level system, the highest level of $E_3$ together with the base level $E_1$ forms the transition allowing the absorption of exciting radiation. After $E_3$ excitation, the quantum system is ideally switched to $E_2$ immediately. Thus, the $E_3$ level is practically zero, and since it does not directly participate in the amplification of the signal, it is not considered in the model described below.

For $N_3 = 0$

$$\frac{dN_2}{dt} = W_pN_1 + W_aN_1 - W_2N_2 - W_eN_2 \quad (7)$$

$$N_{tot}^{Er+Yb} = N_1 + N_2 = N_{tot} \quad (8)$$

### 3.4 Equation of propagation in waveguide

Propagation of the optical signal radiation

$$\frac{dI_S}{dz} = I_s\,(\sigma_e(\nu)N_2 - \sigma_a(\nu)N_1) \qquad (9)$$

Propagation of pumping radiation

$$\frac{dI_p(z)}{dz} = \sigma_a(\nu)N_1 I_p \qquad (10)$$

The calculation of the amplification of the optical active waveguide essentially resides in the solution of the system of differential equations describing the occupation of atomic levels (the so-called rate equations) and in the solution of propagation of light by the propagation equation.
In addition, the resulting relationships for calculating the waveguide gain *G(λ)* are given depending on its length *L* and the required pumping power $P_\lambda(z)$ that, were derived from rate equations (1) – (3) under certain simplified assumptions, where $N_t$ is average concentration of electrons

$$\frac{N_2}{N_t} = \frac{\sum_{\lambda}\frac{P_\lambda(z)\alpha_\lambda}{h\nu\xi}}{1+\sum_{\lambda}\frac{P_\lambda(z)\,(\alpha_\lambda+g_\lambda)}{h\nu\xi}} \qquad (11)$$

$$\alpha_\lambda = \sigma_{a,\lambda}\Gamma_\lambda N_t\,,\; g_\lambda = \sigma_{e,\lambda}\Gamma_\lambda N_t \qquad (12)$$

$\alpha_\lambda$ , $g_\lambda$ are attenuation and gain coefficients
The saturation parameter is defined

$$\xi = \frac{P_\lambda^{sat}(\alpha_\lambda + g_\lambda)}{h\nu} \qquad (13)$$

where

$$P_\lambda^{sat} = \frac{h\nu\pi b^2}{\Gamma_\lambda(\sigma_{e,\lambda}+\sigma_{a,\lambda})} \qquad (14)$$

Waveguide gain in dB can be expressed by attenuation and gain coefficients (15)

$$G_{dB}(\lambda) = 10\,log_{10}(e)\cdot[(\alpha_\lambda + g_\lambda)\frac{N_2}{N_t} - (\alpha_\lambda + \alpha_{\lambda 0})]L \qquad (15)$$

The gain of the waveguide expressed by the *Wa ,We, Wp* rate coefficients is given by (16)

$$G_{dB}(\lambda) = 10\,log_{10}(e)\cdot[(\alpha_\lambda + g_\lambda)\frac{W_a + W_p}{\frac{1}{\tau_2}+W_p+W_a+W_e} - (\alpha_\lambda + \alpha_{\lambda 0})]L \qquad (16)$$

### 3.5 Rate equations for Er and BAC-Ge three-level system

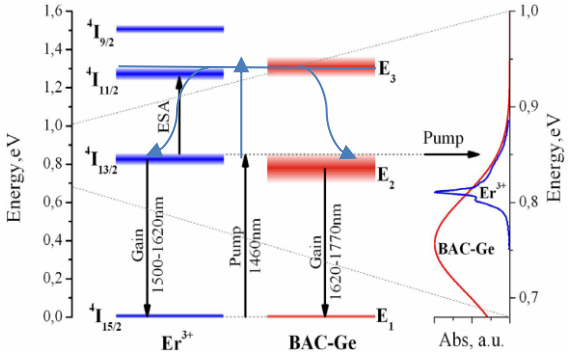


Fig. 11. Energetic levels of $Er^{3+}$ and BAC-Ge (left), absorption bands $Er^{3+}$ and BAC-Ge (right).[3]

The Er and BAC-Ge complex can roughly be described as a three-level quantum system using rate equations in the form:

$$\frac{dN_3}{dt} = -W_{32}N_3 - W_{31}N_3 + W_p N_1 \qquad (17)$$

$$\frac{dN_2}{dt} = W_{32}N_3 - W_2N_2 - W_{eEr}N_2 - W_{eBAC-Ge}N_2 + \\ + W_{aEr}N_1 + W_{aBAC-Ge}N_1 + W_pN_1 \qquad (18)$$

$$N_{tot}^{Er+BAC-Ge} = N_1 + N_2 + N_3 \qquad (19)$$

where $W_{32}$ is the rate coefficient of non-radiation transition from $E_3$ to $E_2$, $W_{31}$ is the rate coefficient of non-radiation transition from $E_3$ to $E_1$,

$W_2 = \frac{1}{\tau_2}$ is spontaneous emissions, (20)

$W_p = \frac{I_p}{h\nu_p}(\sigma_{pEr} + \sigma_{pBAC-Ge}) = W_{pEr} + W_{pBAC\text{-}Ge} = \frac{I_p}{h\nu_p}\sigma_p$ is the rate coefficient pumped,

$W_{aEr} = \frac{I_s}{h\nu_\lambda}\sigma_{aEr}$ is the rate coefficient of stimulated (21) absorption Er,

$W_{aBAC-Ge} = \frac{I_s}{h\nu_\lambda}\sigma_{aBAC-Ge}$ is the rate coefficient of (22) stimulated absorption BAC-Ge,

$W_{eEr} = \frac{I_s}{h\nu_\lambda}\sigma_{eBAC-Ge}$ is the rate coefficient of stimulated emission Er, (23)

$W_{eBAC-Ge} = \frac{I_s}{h\nu_\lambda}\sigma_{eBAC-Ge}$ is the rate coefficient of stimulated emission BAC-Ge.

To calculate the emission effective cross-sections of BAC, Fuchtbauer-Ladenburg suggested a relationship [2].

$$\sigma_{eBAC-Ge} = \frac{\lambda}{4\pi n^2\,\tau\Delta V}\left(\frac{ln2}{\pi}\right)^{1/2} \qquad (24)$$

where
λ is the central wavelength of the BAC emission band
ΔV is the width of the BAC emission band
τ is the lifetime of BAC luminescence
N is the core refractive index of the waveguide core (n = 1.49)

As in the previous case, it is possible to write for the gain of active waveguide doped by Er and BAC-Ge. For $Er^{3+}$ is gain given (25)

$$G_{dB}(\lambda Er) = 10log_{10}(e)\cdot[(\alpha_{\lambda Er} + g_{\lambda Er})\frac{N_2}{N_t} - (\alpha_{\lambda Er} + \alpha_{\lambda 0Er})]L \qquad (25)$$

when we introduce the rate coefficients apply $W_{aEr}, W_{eEr}$, $W_{pEr}$ we get the expression (26)

$$G_{dB}(\lambda)_{Er} = 10\,log_{10}(e)\cdot[(\alpha_{\lambda Er} + g_{\lambda Er})\frac{W_{aEr}+W_{pEr}}{\frac{1}{\tau_2}+W_{pEr}+W_{aEr}+W_{eEr}} - (\alpha_{\lambda Er} + \alpha_{\lambda 0Er})]L \qquad (26)$$

For BAC - Ge is gain given by (27)

$$G_{dB}(\lambda)_{BAC-Ge} = 10\,log_{10}(e)\cdot[(\alpha_{\lambda BAC-Ge} + g_{\lambda BAC-Ge})\frac{N_2}{N_t} - (\alpha_{\lambda BAC-Ge} + \alpha_{\lambda 0BAC-Ge})]L \qquad (27)$$

when we introduce the rate coefficients apply $W_{aBAC-Ge}$, $W_{eBAC-Ge}$ , $W_{pBAC-Ge}$ we get the expression (28)

$$G_{dB}(\lambda)_{BAC-Ge} = 10\, log_{10}(e)\cdot [(\alpha_{\lambda BAC-Ge} + + g_{\lambda BAC-Ge}) \frac{W_{aBAC-Ge} + W_{pBAC-Ge}}{\frac{1}{\tau_2} + W_{pBAC-Ge} + W_{aBAC-Ge} + W_{eBAC-Ge}} - - (\alpha_{\lambda BAC-Ge} + \alpha_{\lambda 0BAC-Ge})]L \quad (28)$$

These relationships apply only approximately, the exact solution requires a numerical solution of the mathematical model. However, the approximate solutions and simplicity of the calculation are very useful.

## 3. Conclusion

Measurements were experimentally proved option to create optical active structure in telecommunication band C + L + U (1530 - 1675 nm). Further, a simplified mathematical model for Er + Yb structures and Er + BAC-Ge structures was described.

Despite these advances in the development of optical active bizmuth/erbium doped waveguides, many fundamental scientific and technological issues and challenges remain unsolved. One major challenge is to explain the nature of the emission of active bismuth centers (BACs). So far, several origins of NIR emissions have been suggested in bismuth-doped glasses, but none have been directly confirmed. Another problem consists that bismuth is a transition metal with d-orbitals, which easily associate with the surrounding environment (matrix), in contrast to rare earth atoms that f - orbitals are well isolated (shielded). This binding to the external environment generates broadband emission defects. There are a number of other issues such as low draw efficiency, strong and wide ESA, etc.

After solving these and many other problems, however, bizmuth/erbium doped waveguides can be a solution new generation broadband applications. In our further research we will focus on this wavelength range (1500-1700 nm), for telecommunication applications in the third optical attenuation window of silica waveguides. In this area of wavelengths, we want to develop a planar active optical waveguide, for L – U telecommunication band and a mathematical model to optimize a technological parameter.

**ACKNOWLEDGMENT**

Our research is supported by the Student Grant Competition of the Czech Technical University in Prague under grant number SGS18/139/OHK3/2T/13.

## REFERENCES

[1] Binbin Yan, Yanhua Luo, Amirhassan Zareanborji, Gui Xiao, Gang-Ding Peng and Jianxiang Wen "Performance comparison of bismuth/erbium co-doped optical fiber by 830 nm and 980 nm pumping" Jurnal of Optics 18, (2016), pp.1-8

[2] Qiancheng Zhao,Yanhua Luo,Wenyu Wang,John Canning, and Gang-Ding Peng,"Enhanced broadband near-IR Luminescence and gain spectra of bismuth/erbium co-doped fiber by 830 and 980 nm dual pumping" AIP Advances 7, (2017), 045012 1-8

[3] S V Firstov, K E Riumkin, A M Khegai, S V Alyshev, M A Mekumov, V F Khopin, F V Afanasiev and E M Dianov "Widebannd bismuth and erbium codoped optical fieber amplifier for C + L + U telecommunication band" Laser Phys.Lett. 14, (2017), pp. 1-5.

[4] Murata K, Fujimoto Y, Kanabe T, Fujita H and Nakatsuka M „Bi-doped SiO2 as a new laser material for an intense", Laser Fusion Eng. Des., (1999), 44 437–9.

[5] Smejcky J., Jerabek V., Nekvindova P." Gain Determination of Optical Active Doped Planar Waveguides", Conference on Photonics, Devices, and Systems VII , Prague, AUG 28-30,2017,Proceedings of SPIE Volume: 10603, Article 106030P.

[6] Smejcky, J. Jerabek, V.; Nekvindova, Wideband Bismuth - Erbium Doped Optical Active Planar Waveguides, Proceedings of OK 2018, Prague, pp. 41.

# Optimization and Investigation of Fiber to Chip Butt Coupler for SiN Integrated Photonics

Jozef Chovan [1], František Uherek [1, 2], Dana Seyringer [3], Lenka Gajdošova [3],
Eduard Koza [4], Jozef Pavlov [4]

[1] *International Laser Centre, Ilkovičova 3, 841 04 Bratislava*
[2] *Faculty of Electrical Engineering and Information Technology, Slovak University of Technology, Ilkovičova 3, 812 19 Bratislava*
[3] *Research Centre for Microtechnology, Vorarlberg University of Applied Sciences, Hochschulstr. 1, 6850 Dornbirn, Austria*
[4] *Sylex, s.r.o., Mlynské Luhy 53, 821 05 Bratislava*

***Abstract*— The paper deals with the optimization and investigation of fiber to SiN optical chip butt coupler with single step fabrication process without thickness tapering of the waveguide layers. Coupler is designed for 850nm band for coupling between strip 0.25 μm x 1.00 μm SiN waveguide and Nufern's 780-OCT single mode optical fiber with core diameter 4.4 μm. The layout of the butt coupler is optimized for minimal coupling losses. The coupling losses and their spectral and displacement sensitivities are simulated and investigated. The two simulation methods, finite-difference beam propagation techniques and eigenmode expansion method, are used.**

***Index Terms* — silicon nitride, rib waveguide, power splitter**

## I. INTRODUCTION

SILICON nitride (SiN) is a common material in CMOS technology and it is typically deposited by either Low Pressure Chemical Vapour Deposition (LPCVD) at high temperature (>700 °C) or by Plasma Enhanced Chemical Vapour Deposition (PECVD) at low temperature (<400 °C). LPCVD-based SiN is typically close to stoichiometric $Si_3N_4$, it is highly strained and provides an excellent control over the homogeneity of material refractive index and thickness. It has a refractive index of around 2.0 at a wavelength of 1550 nm. PECVD-based SiN has a composition that depends strongly on the deposition conditions and can be silicon-rich (higher refractive index) or nitrogen-rich (lower refractive index). Both types of nitride have been used for photonic ICs. To this end the LPCVD nitride is annealed at high temperature to drive out the hydrogen [1]. SiN is transparent throughout most of the visible spectral range (down to at least 500 nm) and therefore, it is a viable candidate to implement "silicon photonics" at wavelengths below 1.1 μm. SiN waveguides on silicon find applications in communication, signal processing, optical sensors, narrow-band filters, photonic band gap engineering, on-chip optical frequency comb generation, short pulse generation and photonic integrated circuits for optical interconnects [2-5].

The paper presents the optimization and investigation of the fiber to SiN chip butt coupler with single step fabrication process without thickness tapering. Coupler is designed for 850 nm band with coupling between strip 0.25 μm x 1.00 μm waveguide and Nufern's 780-OCT single mode optical fiber with core diameter 4.4 μm [6]. The coupling losses simulation results of the two simulation methods finite-difference beam propagation techniques (Synopsys BeamPROP) and eigenmode expansion method (Synopsys ModePROP) are compared. Spectral and displacement sensitivities of coupling losses are simulated and investigated by eigenmode expansion method.

## II. DESIGN, SIMULATION AND OPTIMIZATION

The designed, optimized and investigated photonic structure is consisted of a silicon substrate, a 10 μm thick thermal $SiO_2$ layer with a refractive index of 1.456, a 0.25 μm thin PECVD SiN layer with refractive index of 1.88 at 850 nm and a 1.5 μm PECVD SiOx passivation layer with a refractive index of 1.48. We are assuming the strip waveguide with width 1 μm in this design. The contour map of transverse index profile of this strip waveguide structure is shown in Fig. 1. This single mode strip waveguide is used as input waveguide of the SiN chip. In the coupling loss evaluation, we are using two monitor areas for calculation of optical power coupled into the SiN waveguide due to evanescent field of waveguide. The first one is exact area of the strip waveguide with dimensions 0.25 μm x 1.00 μm and second one is area including evanescent field of waveguide. The second monitor area we assume 3 times thickness and 1.5 times width of strip waveguide (0.75 μm x 1.50 μm) with center point in the middle of strip waveguide.

The main idea of this fiber to chip coupler design is used the low-contract refractive index waveguide created from $SiO_x$ passivation layer and $SiO_2$ buffer layer covered by air for coupling optical radiation to and from the optical fiber in combination with inverse taper of SiN waveguide. The contour map of transverse index profile of the low-refractive index contrast waveguide is shown in Fig. 2. The waveguide is created by etching whole 1.5 μm passivation PECVD $SiO_x$ layer and partial etching of the buffer layer thermal $SiO_2$ into 1.5 μm deep. The created waveguide has square profile with 3 μm x 3 μm dimensions. The fundamental mode is standing at the top of the created waveguide due to higher value of the $SiO_x$ passivation layer refractive index in comparison to thermal $SiO_2$ buffer layer. The cross-section of the designed

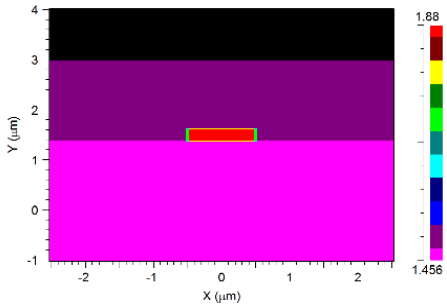


Fig. 1. Contour map of transverse RI profile of SiN strip waveguide.

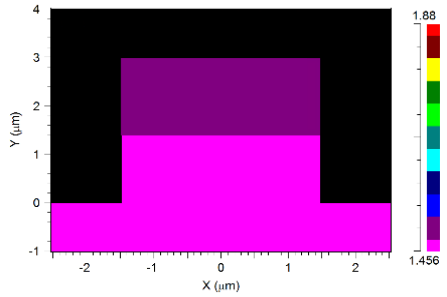


Fig. 2. Contour map of transverse RI profile of SiN strip waveguide.

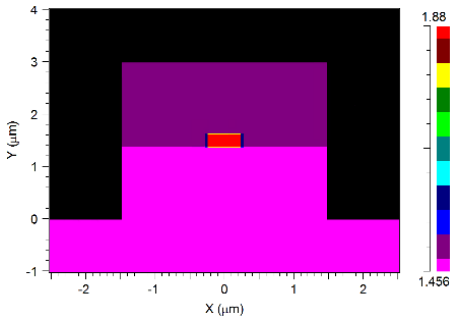


Fig. 3. Contour map of transverse RI profile of SiN strip waveguide.

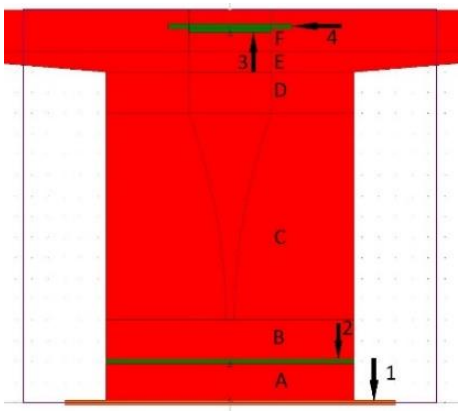


Fig. 4. Top view of the designed coupler.

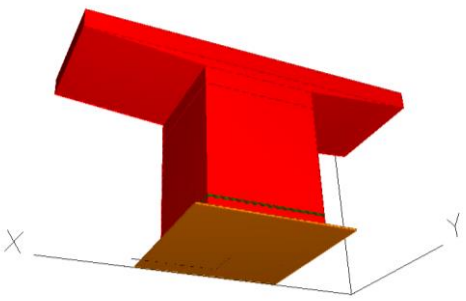

Fig. 5. 3D view of the designed coupler.

coupler at the inverse taper section is shown in Fig. 3. There is the SiN waveguide with width less than standard waveguide width 1 µm used at whole SiN chip. SiN waveguide is placed at center of the low-contract RI waveguide. The fundamental mode shape is transforming from elliptical to round and the fundamental mode diameter is increasing by the inverse taper section in waveguide to fiber direction. In opposite direction from fiber to waveguide the diameter of fundamental mode is decreasing and fundamental mode round shape is transform to elliptical by the inverse taper section. The top - view of the designed butt fiber to chip coupler is shown in Fig. 4. This top - view is not a scale due to all coupler parts visualization possibilities. Letters A – F indicate each sections of the designed coupler. Numbers indicate the launch field and power monitors in simulations. Fig. 5 shows the 3D view of the designed coupler exported from simulation tools. Section A is low-contract refractive index waveguide section of the designed coupler. The cross-section of this coupler section is shown in Fig. 2. Section B has the same cross-section as section A. It was added into simulation layout for investigation of low-contract refractive index waveguide length influence to overall coupling losses. The investigation showed that length of the section B has not significant influence to overall coupling losses. In the final design 10 µm lengths of section A and B were used. Section C is inverse taper section of the designed coupler. The height 0.25µm of the SiN waveguide is not changing in this section, but the width of the SiN waveguide is changing exponentially. The shape and dimensions in final coupler design of the low-contrast refractive index waveguide which covers the SiN waveguide is not changing in this section C. In initial phase of coupler design the influence of this waveguide shape to overall coupling losses was studying, but it has not significant influence. The cross-section of this coupler section C at some inside section position is shown in Fig. 3. All three sections D, E and F of coupler have the full profile SiN waveguide 0.25µm x 1.00µm. What is different on these three sections is the shape of cover low-contrast refractive index waveguide. Section D has low-contrast refractive index waveguide as previous sections A, B, and C. In the section E low-contrast refractive index waveguide is disappearing and standard SiN chip waveguide structure is starting. Section F is the standard SiN chip waveguide structure. The cross-section of this standard SiN chip waveguide structure is shown in Fig. 1. Number 1 in Fig. 4 shows to fiber mode launch field with diameter 4.4 µm x 4.4 µm. Launch field was placed at the beginning of coupler section A without airgap and with 2 µm airgap in direction from optical fiber to SiN waveguide. Number 2 in Fig. 4 indicates the position of the monitor No. 1 with dimensions of the low-contract refractive index waveguide 3 µm x 3 µm. The 2D $E_x$ profile of TE fundamental mode at this monitor No. 1 position is shown in Fig. 6. Values in x and y axes in Figs. 6 – 8 are relative coordinates to point shown at top of each Fig. Monitor No. 1 indicates the coupling losses between optical fiber and low-contract refractive index waveguide. The fundamental mode in the low refractive index contrast waveguide is located at top part of the waveguide due to the sandwich structure with higher refractive index layer at the top of the waveguide.

Number 3 in Fig. 4 shows to monitor No. 2, which is placed in the center of SiN strip waveguide and has the same dimensions as SiN waveguide part 250 μm x 1000 μm. This monitor gives exact value of the optical power coupled into SiN waveguide part without evanescent field. The 2D $E_x$ profile of TE fundamental mode at monitor No. 2 position is shown in Fig. 7. Mode profile has big evanescent field and only part of the coupled power into SiN is evaluated by this monitor. Number 4 in Fig. 4 shows the position of next monitor No. 3, which has 3 times higher thickness and 1.5 times larger width of strip SiN waveguide (0.75 μm x 1.50 μm) and it is placed in the center point of strip SiN waveguide. This monitor gives value of the optical power coupled into SiN waveguide including evanescent field. The 2D $E_x$ profile of TE fundamental mode at this monitor is shown in Fig. 8. Fig. 8 represent the integration area for evaluation of optical power of fundamental TE mode by monitor No. 3. This area covered the main parts of the fundamental mode profile.

The simulation of optical power coupling from optical fiber to SiN waveguide as a function of the tip width of the SiN waveguide at the beginning of inverse taper section C for TE polarization was done with two simulation methods:

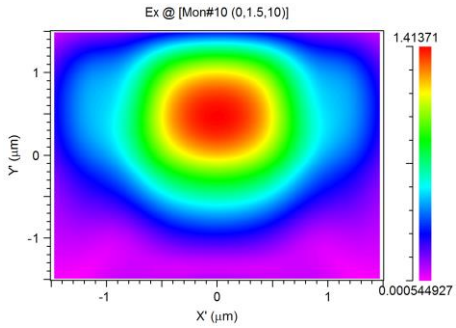


Fig. 6. 2D $E_x$ profile of TE fundamental mode at monitor No.1 position.

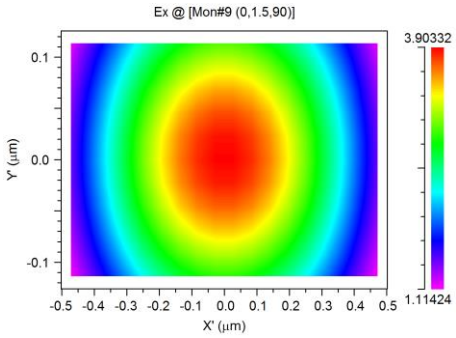


Fig. 7. 2D $E_x$ profile of TE fundamental mode at monitor No. 2 position.

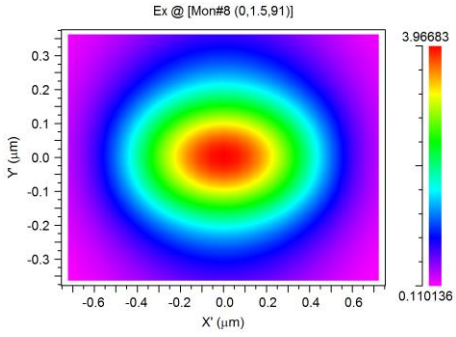


Fig. 8. 2D $E_x$ profile of TE fundamental mode at monitor No. 3 position.

BeamPROP (finite - difference beam propagation techniques) and ModePROP (eigenmode expansion method). These simulation results are shown in Fig. 9. There are 3 lines for BeamPROP simulations and 3 lines for ModePROP simulations. The ModePROP method is more suitable and accurate method than BeamPROP for this type simulation but it is also several times more time and RAM consumable. Due to this fact the steps of simulation of ModePROP are coarse. The simulation results from these two simulation methods correspond together and they have the same behavior on changing parameters of the coupler. The absolute value of simulated coupled powers is different up to 25%. Due to this fact, the investigation and optimization of the designed coupler was done by BeamPROP method, which is less time consumable, but the final values of the coupling losses of the final coupler topology was done by more accurate ModePROP method. The beginning tip width of the SiN waveguide has dominant effect to overall coupling losses. For coupling efficiency more than 90% the tip width should be less than 0.1 μm. In the final design we used the 0.1μm value of the tip width.

The influence of the inverse taper section C length to overall coupling losses was also investigated by ModePROP method. The simulations were done for inverse taper section C length in the range 20 μm - 300 μm. Coupling efficiency was increasing in the range from 20 μm to 50 μm, but the next increasing of inverse taper section C length was not increasing the coupling efficiency dramatically. Due to this fact in the final coupler design the 50 μm of inverse taper section C length was used.

$E_x$ mode profiles over Z axis of the final coupler design simulated by ModePROP tools are shown in Fig. 9. Coupler section A and B have 10 μm length each, C section has 50 μm and sections D, E, F have together 25 μm length. The overall coupler length is 95 μm. In comparison to previously

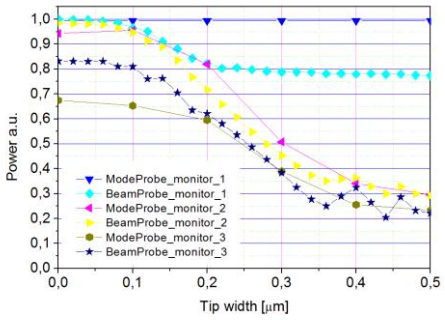


Fig. 9. Optical power coupled into SiN waveguide as a function of SiN waveguide tip width at the beginning of inverse taper C section of coupler for TE polarization.

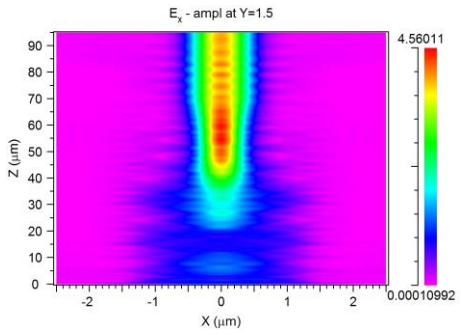


Fig. 10. 2D $E_x$ profile of TE fundamental mode over Z axis

published Fiber-to-Waveguide Coupler [7] for SiN waveguide, which has 500 µm adiabatic taper and 300 µm end waveguide, our designed fiber to chip butt coupler is more than 8 times shorter and takes much less space on the SiN chip.

## III. Simulation and Investigation

The XY alignment tolerance and spectral band of designed fiber to chip butt coupler were simulated and investigated. The displacement of fiber to chip coupler were simulated over the range from -1.5 µm to 1.5 µm in X and Y axes relatively to central point of the low refractive index contrast waveguide of the coupler. The Fig. 11 (y axis displacement) and Fig. 12 (x axis displacement) show the simulation results for three different power monitor over Z axis. The power monitors are the same as in previous paper section. The alignment 1dB tolerance band for Y axis is more than 1.5 µm and for X axis is more than 2.5 µm. For X axes displacement the maximum of coupling efficiency is achieved at central point of low contrast refractive index waveguide but for Y axis displacement the maximum of coupling efficiency is achieved at 0.38 µm above the central point of the low contrast refractive index waveguide. This is cause by sandwich structure of low refractive index contrast waveguide with higher refractive index layer at the top of the waveguide.

Fig. 13 show the total transmitted, reflected and absorbed power simulated by ModePROP tool over simulated spectral range from 600nm to 1000nm. The launch and reflection planes in Z axis are placed at the beginning of simulation domain and transmission plane is placed at the end of simulation domain. Over the simulated spectral range, the values of the simulated parameters are changing in the range less than 10% without any resonant effect. The transmission of the whole coupler structure is more than 82%.

Fig. 14 shows the simulation results of the optical power coupling into SiN waveguide as a function of wavelength. The simulation is done for all three power monitors. The coupled optical power into SiN waveguide including evanescent field (power monitor 3) is changing value in whole simulated spectrum band 400 nm no more than 1 dB.

Simulated and calculated coupling losses of the final coupler design done by ModePROP tools are listed in Tab. 1. Simulations were done for two type interface between fiber and SiN waveguide chip. The first one is without airgap and the second one is with 2 µm airgap between fiber and SiN chip. The calculations of the coupling losses were done for three different positions and areas in the coupler. First position is at low contract waveguide marked by number 2 in Fig. 4 and area is whole low contract waveguide 3 µm x 3 µm. It represents coupling losses between optical fiber and low contract refractive index waveguide. The second position is at SiN strip waveguide marked by number 4 in Fig. 4 over SiN waveguide area including evanescent field 0.75 µm x 1.50 µm. The third position is at SiN strip waveguide marked by number 3 in Fig. 4 over only exact SiN waveguide area 0.25 µm x 1.00 µm. It represents coupled optical power into SiN waveguide excluding evanescent

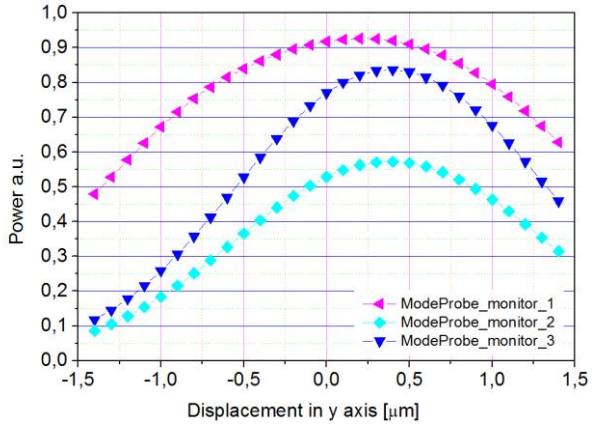


Fig. 11. Optical power coupled into SiN waveguide as a function of fiber displacement in y axis.

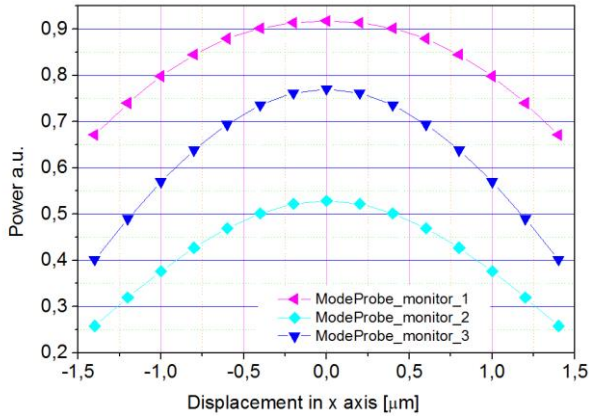


Fig. 12. Optical power coupled into SiN waveguide as a function of fiber displacement in x axis.

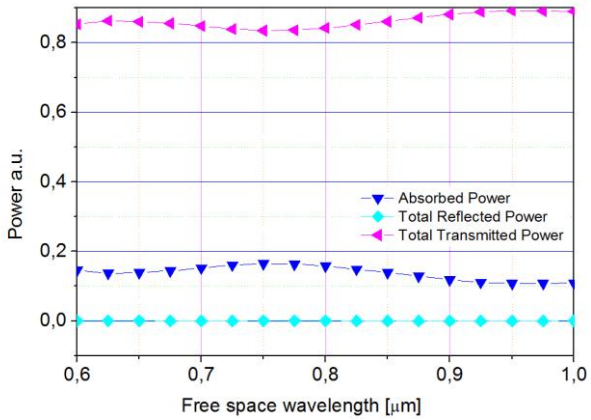


Fig. 13. Total transmitted, reflected and absorbed power.

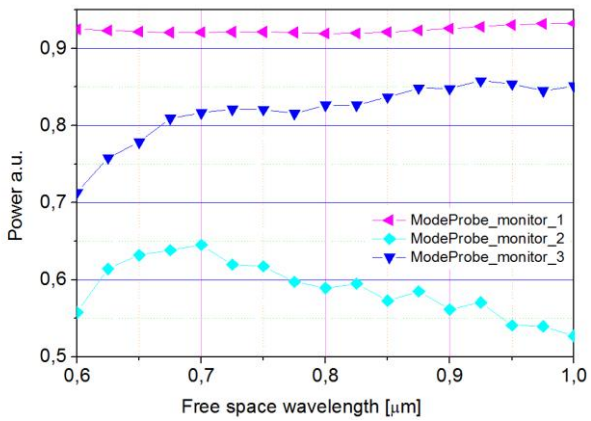


Fig. 14. Optical power coupled into SiN waveguide as a function of wavelength.

TABLE I.
SIMULATED AND CALCULATED COUPLING LOSSES BETWEEN NUFERN'S 780-OCT SINGLE MODE OPTICAL FIBER AND SIN STRIP WAVEGUIDE BY MODEPROP TOOL.

| Parts of coupler | Fiber to chip interface | Power [a.u.] | Coupling losses [dB] |
|---|---|---|---|
| Low contract waveguide | without air gap | 0,92 | 0,36 |
| | with air gap | 0,84 | 0,74 |
| SiN waveguide including evanescent field | without air gap | 0,84 | 0,77 |
| | with air gap | 0,77 | 1,12 |
| SiN waveguide excluding evanescent field | without air gap | 0,57 | 2,42 |
| | with air gap | 0,53 | 2,78 |

field. Our designed butt coupler has 0.77 dB coupling losses including and 2.42dB excluding the evanescent field of SiN waveguide at 850nm band without air gap at fiber to chip interface. Values of coupling losses are higher in the case of existing airgap between fiber and SiN chip.

## CONCLUSION

In the paper the simulations, optimization and investigation of the fiber to SiN chip butt coupler with single step fabrication process without thickness tapering are reported. Coupler was designed for 850 nm spectral band for coupling between Nufern's 780-OCT single mode optical fiber with core diameter 4.4 μm to strip 0.25 μm x 1.00 μm SiN waveguide. The coupling losses simulation were performed by two simulation methods: finite-difference beam propagation techniques and eigenmode expansion method and simulated results are compared. The overall optimized coupler length is 95 μm. Optimized butt coupler has 0.77 dB coupling losses including and 2.42dB excluding the evanescent field of SiN waveguide at 850nm spectral band without air gap at fiber to chip interface. The 1dB operation spectral band of the optimized coupler is more than 400 nm. The alignment 1dB tolerance band of the coupler for Y axis is more than 1.5 μm and for X axis is more than 2.5 μm.

## ACKNOWLEDGMENT

Work was supported by projects 1/0929/17 of VEGA grant agency of Ministry of Education, Science, Research and Sport of the Slovak Republic, projects SK-AT-2017-0005, APVV-17-0662 from Slovak research and development agency of Ministry of Education, Science, Research and Sport of the Slovak Republic and SK 15/2018 from Austrian Agency for International Cooperation in Education and Research (OeAD-GmbH).

## REFERENCES

[1] R. Baets et all., In *Proceedings of OFC 2016*, Anaheim, CA, USA, Th3J.1 (2016).

[2] M. J. Heck, J. F. Bauters, M. L. Davenport, D. T. Spencer, and J. E. Bowers, "Ultra-low loss waveguide platform and its integration with silicon photonics," Laser & Photonics Reviews, vol. 8, no. 5, pp. 667–686, 2014.

[3] D. J. Moss, R. Morandotti, A. L. Gaeta, and M. Lipson, "New cmos-compatible platforms based on silicon nitride and hydex for nonlinear optics," Nature Photonics, vol. 7, no. 8, pp. 597–607, 2013.

[4] H. Yu, M. Chen, Q. Guo, M. Hoekman, H. Chen, A. Leinse, R. G. Heideman, R. Mateman, S. Yang, and S. Xie, "$Si_3N_4$-based integrated optical analog signal processor and its application in rf photonic frontend," Photonics Journal, IEEE, vol. 7, no. 5, pp. 1–9, 2015.

[5] L. Zhuang, D. Marpaung, M. Burla, W. Beeker, A. Leinse, and C. Roeloffzen, "Low-loss, high-index-contrast si 3n4/sio 2 optical waveguides for optical delay lines in microwave photonics signal processing," Optics express, vol. 19, no. 23, pp. 23 162–23 170, 2011.

[6] https://www.nufern.com/pam/optical_fibers/2587/780_nm_Dispersion_Controlled_Select_Cutoff_Fiber/

[7] Zhu, T., Hu, Y., Gatkine, P., Veilleux, S., Bland-Hawthorn, J., & Dagenais, M., "Ultra-broadband High Coupling Efficiency Fiber-to-Waveguide Coupler Using $Si_3N_4/SiO_2$ Waveguides On Silicon", October 2016, IEEE Photonics Journal Vol. 8 (No. 5): 1-1 DOI: 10.1109/JPHOT.2016.2600037

# Bi-Directional Erbium-Doped Frequency Amplifier test facility for long distance transmissions in C-Band and L-Band

Sarbojeet Bhowmick[1], Josef Vojtech[1] and Radek Velc[1]
Email: josef.vojtech@cesnet.cz, sarbojeet@cesnet.cz, radek@cesnet.cz
*CESNET, Prague, Czech Republic[1]*

***Abstract*— Erbium-Doped Frequency Amplifier (EDFA) is an optical amplifier operating in both C-Band and L-Band. Such EDFA use in C-band and L-band minimize the problems like insertion loss and dispersion, and that can be utilized in long-distance optical fiber links. Optical fiber amplifiers make efficient amplification of optical signals leading to amplified spontaneous emission of photons by rare metal ions present in the optical fiber. We establish an incredible technique using Czech Light™ Erbium-Doped Frequency Bi-Directional Amplifier (CLA BiDi) for an ultra-stable coherent optical frequency transfer in both C-band and L-band with an input signal-20dB. Amplifiers of such conditions generally use for WDM transmissions having relatively flat gain.**

***Index Terms*—optical amplifier, insertion loss, amplification, rare metal ions, ultra-stable coherent, optical frequency transfer, flat gain.**

## I. Introduction

A PROCEDURE to exhibit the characterization of bidirectional optical amplifier used for very long distance transmission, eventually in the systems of the Wavelength-Division Multiplexing (WDM) is presented. An EDFA is now most commonly used to compensate the loss of an optical fiber in long-distance optical communication. EDFA can amplify multiple optical signals simultaneously, which leads to Wavelength-Division Multiplexing (WDM) technology [4]. EDFA optical characteristics are mainly: 1) High output power from an amplifier when sufficient signal input power (0dBm or higher) is launched to the amplifier. A booster amplifier works under this condition. 2) Small-signal gain in an amplifier, when the signal power launched to the amplifier is very small (in this experiment it is approximately -20dBm). A pre-amplifier operates under this condition and a small signal gain is an important characteristic for a pre-amplifier. 3) Noise figure of an optical EDFA amplifier adds some noise to the original signal because an Amplified Spontaneous Emission (ASE) from the EDFA leads to decrease the Optical Signal-to-Noise Ratio (SNR). ASE grows fast when the signal input power is low. 4) An optical EDFA amplifier is used for WDM transmission, with all WDM channels considering equal gain in ideal case. Gain flatness is a factor where many EDFAs are concatenated in an optical transmission line where the signal gain variation is gathering the EDFA chains and that leads to large signal power differences between the WDM channels. However, the main goal of our experiment was to verify spectral dependence of amplifier gain and noise figure using Tunable Laser source.

This work was supported partially by the Ministry of Education, Youth and Sport of the Czech Republic as part of the CESNET E-infrastructure project LM2015042 and by the project "E infrastructure CESNET - modernization", reg.nr. CZ.02.1.01/0.0/0.0/16_013/0001797.

## II. Mathematical views and experimental setup

### A. Proposed Methodology

Gain in optical amplifiers produced by stimulated emission always guided by spontaneous emission. Gain means the ratio of the output signal power to the input signal power.

$$\text{Gain (in dB)} = 10 \log_{10} \frac{P_{out}}{P_{in}} \quad \ldots(1)$$

(From Reference 8)

Here, $P_{out}$ and $P_{in}$ is the output and input signal power of EDFA.

When spontaneously emitted photons are captured and accompanied in the optical fiber core, they induce stimulated emission and are amplified which gives rise to amplifier spontaneous emission (ASE). Gain of EDFA depends on the pump power as well as on the pump wavelength. As the pump power increases, the gain becomes roughly independent of pump wavelength. Gain flattening [1] is required if EDFAs are to be cascaded. Relative flat gain greater than 20 dB is useful for WDM applications.

Gain in EDFA is achieved due to population inversion of dopant ions. As there we know limited number of dopant ions, increasing pumping power to a level at which all the dopant are excited will not increase the population of the excited level any further and the gain saturation will take place. The behavior is different from that of electronic amplifier where the gain curve is linear till saturation abruptly occurs. This results in signal distortion for an electronic amplifier that is operated near saturation point.

Noise Figure (NF) is a measure of the quality of amplification. It is defined as the quotient of the signal OSNR of the input signal to that of the output signal.

$$\text{NF (in dB)} = 10 \log_{10} \frac{(OSNR)_{input}}{(OSNR)_{output}} \quad \ldots (2)$$

(From Reference 8)

We get, $(OSNR)_{input}$ is signal-to-noise ratio of the input signal and $(OSNR)_{output}$ is signal-to-noise ratio of the output signal.

Due to amplified spontaneous emission (ASE), the output OSNR is smaller than that of the input and hence NF > 1 i.e., an optical amplifier cannot improve the optical signal OSNR.

Erbium-Doped Fiber Amplifier (EDFA) is used in this experiment for C/L-band and L-band. The propagation equations [8], which give the signal, pump and ASE variations along the fiber, depend also on the pumping scheme. The variation of gain with fiber length for pump powers having a constant signal input power and erbium doping density. The gain increases up to a certain length of fiber, and then begins to decrease after a maximum point. The reason for the decrease in gain is insufficient population inversion due to excessive pump depletion and getting higher losses than the provided gain at the signal wavelength due to high total loss of Erbium doped fiber (fiber background loss $Er^{+}$ absorption loss).

### *B. Experimental Setup*

For this experiment, the signal source Tunable Laser and pump laser amplifier Czech Light™ EDFA [2] both in C/L-band and L-band separately used to measure optimum performance of EDF [3]. Figure 1, shows the optical amplifier configuration details. Low-noise signal source Tunable Laser provided by [5] specially used in optical communication connected to 25dB for C/L-band and 20dB for L-band attenuator is then connected to Czech Light™ EDFA [2]. The output of EDFA is connected to Optical Spectrum Analyzer.

Laser noise characteristics in real-time have usual noise from these sources and they will be added to Lorentzian spectrum and leads to a Gaussian distribution. The originality of such setup lies on the technique of getting an ultra-stable frequency signal gain using EDFA Bi-Directional Amplifier.

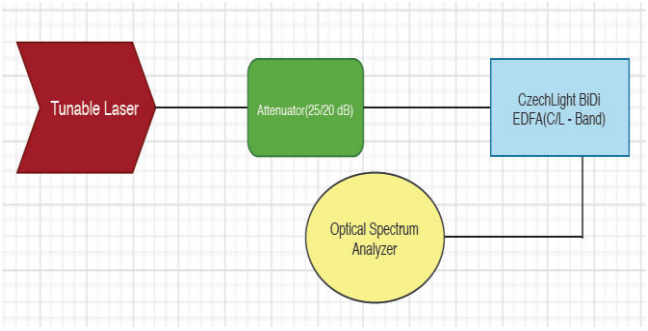


Figure 1: Schema of Hybrid Amplifier (ITLA Pump and Czech Light™ EDFA) under counter-propagation configurations for ITLA and EDF amplifying stages

### *C. Results and Discussion*

The results of this experiment are based on various laser pump current rates. In WDM transmissions, the performance of hybrid amplifier continues to have signal gain. The EDFA pump configuration current rates are measured in different values. In Tunable Laser, the Fine Tune Frequency (FTF) is maintained as 500-1300 kHz. The performance of EDFA using signal source Tunable Laser and Czech Light™ EDFA leads to increase in length of EDF and provides more power. The evaluation of pumping techniques configures the system with gradual improvement and works optimally. The signal gain analysis makes the transmission acceptable.

The signal gain we get from this experiment setup at different power current rates in C/L-Band and L-Band is shown in the below graphs. (Figure 2, Figure 3 and Figure 4)

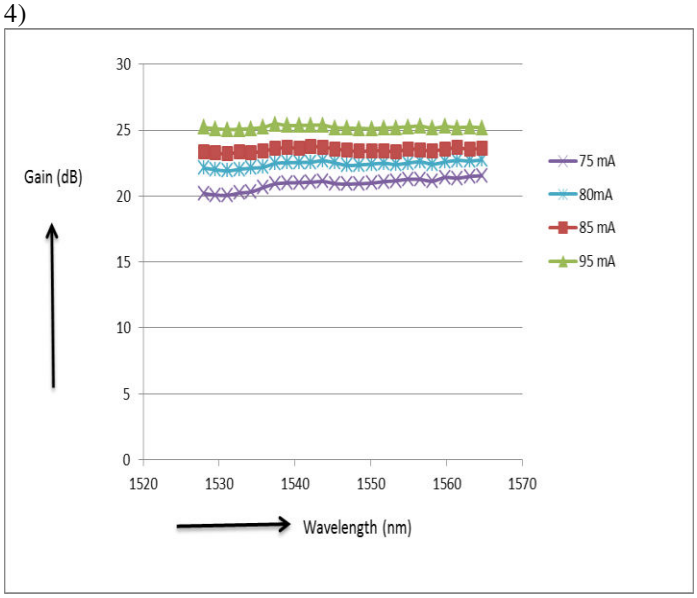


Figure 2: Spectral dependency of amplifier for pump currents in C-Band

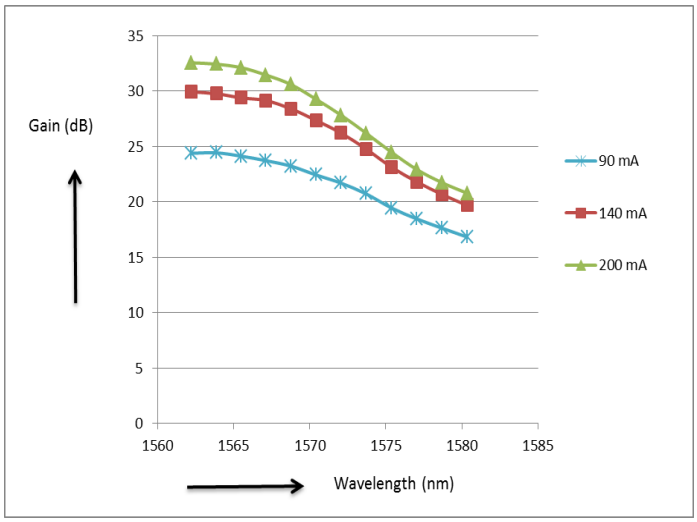


Figure 3: Spectral dependency of amplifier for pump currents in 1570 nm

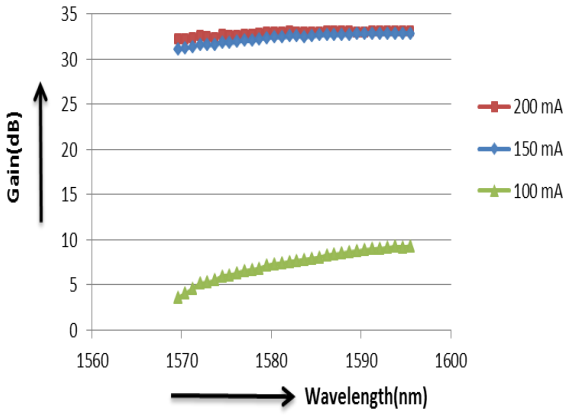


Figure 4: Spectral dependency of amplifier for pump currents in L-Band

In case of ASE noise level the process has been stimulated in gain medium for optical laser configuration system. ASE noise level graph shows the excitation of the gain medium achieved by the ultra-stable coherent laser frequency levels. Figure 5 and 6, shows ASE noise levels at different laser pump rates.

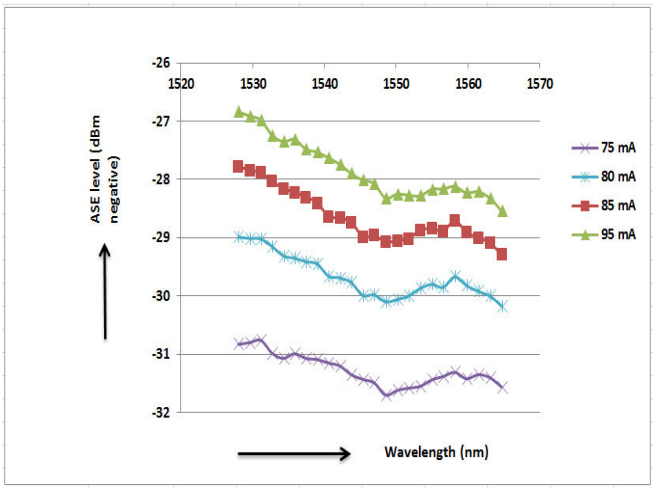


Figure 5: ASE noise level output for EDFA in C-Band

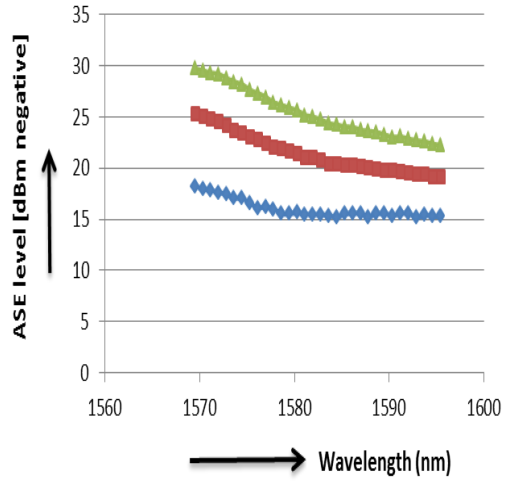


Figure 6: ASE noise level output for EDFA in L-Band

ASE noise level in fiber amplifier tends to limit the gain achievable in a single stage of a fiber amplifier in the order of 20-30dB.

Now OSNR is an essential parameter to find the performance of wavelength-division-multiplexed (WDM) transmission in each channel. OSNR is monitored here by measuring the polarization extinction ratios of WDM transmission. OSNR automatically uses the polarization-nulling method.

EDFA transient gain control performance sometimes specified for stimuli consisting of a linear ramp in input power over 50 or 100 µs. Rare faults, such as a fiber break at a splice can be very fast, sometimes the transient response specified as worst case event " instantaneous transient" which addresses stimuli faster than 1 µs. The optimum fiber length is defined by the fiber length conceived in order to get maximum EDFA gain. It is important in evaluating the EDFA performance using random variation of the input power channels. The gain characteristics of the EDF maintain coupled mode theory that show gain term of the EDF. In EDFA the erbium ions in the metastable level decay to the ground level through stimulated emission by an incoming signal.

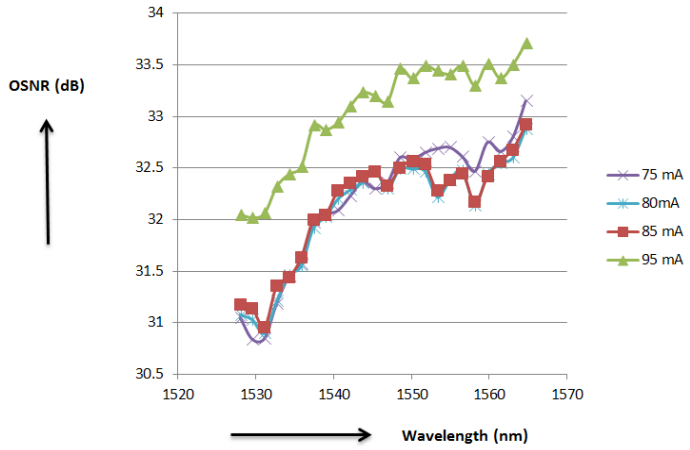


Figure 7: Optical signal-to-noise ratio (OSNR) in C-Band

For the large gain the OSNR is independent of the gain, leads to a useful outcome that controls the system performance of in-line EDFAs.

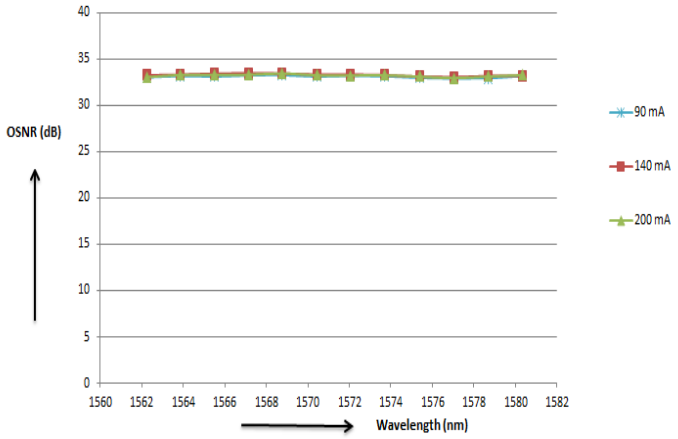


Figure 8: Optical signal-to-noise ratio (OSNR) in 1570 nm

The OSNR is an important design parameter for optically amplified systems. End-to-end system performance can be diagnosed from the OSNR and the model of total noise in the receiver.

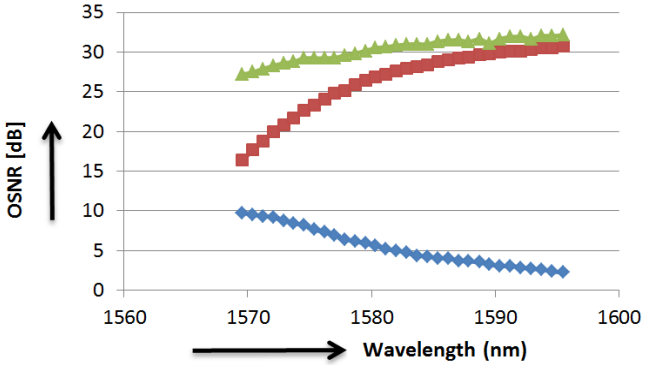


Figure 9: Optical signal-to-noise ratio (OSNR) in L-Band

The lasers were operated at the ITU-standardized with 100 GHz Grid frequencies at 191.00~187.90 THz. The Tunable Laser device first manually fixed the wavelength range for C-Band and then L-band in nanometer (nm) value simultaneously setting the Frequency Fine Tune Set Point (FTF) 0~800MHz is fixed in each case and start to measure the Power gain in Whisper Mode after the laser get reflected back from the Czech Light™ Erbium-Doped Fiber Amplifier (EDFA).

## III. Upcoming goals

Brillouin gain process occurs when light is diffracted backward on the moving grating, giving rise to frequency shifted Stokes and anti-Stokes components. In the optical fibers within this experiment, Brillouin scattering occurs essentially on the backward direction. Brillouin frequency shift basically depends on the material composition and on other quantities as the extent of temperature and pressure of the medium which we get here for fiber-optic sensors.

The Tunable-pump lasers combination produce signal gain profile. In future we will focus to achieve Brillouin gain with setting proper signal and pump offsets focusing several amplifier technologies in metro environment. The work will bring up optical novice interested to get information about this arena leads to get use to framework of reference on what the technology brings up ensuring the cost impact too. The upgradation of firmware for SDN controlled Czech Light™ BiDi EDFA will bring out machine learning approach in optical communications.

## IV. Conclusion

An implementation of measuring an ultra-stable optical coherent frequency has been demonstrated. The use of ID-Photonics™ which is a Continuous Wave Tunable Laser with integrated electronics and the monitoring is fully through digital interface. On the other hand, the Czech Light™ Erbium-Doped Fiber Amplifier (EDFA) based on Czech Light™ Distro 5 for EDFA configuration proved very accurate measurement to obtain power signal gain. Next, we have planning to do the characterization of Brillouin amplifier in near future. For long distance optical signals like this experiment the optical signals are transmitted over Dense WDM (DWDM) which uses large number of channels into the gain bandwidth. The effects of ultra-stable coherent communication applications, the linewidth is important to reduce the phase variation over the duration of 40ps/bit. The power input rates located in one frequency channel [6] help us to gain ultra-stable frequency transfer signal, the other channels carry noise traffic in WDM transmission. Such BiDi Amplifiers are also utilized within CESNET2 network where frequency transmissions are running together with data traffic and other advanced services (sensing) and are currently utilized for e.g. precise measurements of nuclear power plant containment stability. Project CLONETS [7] targets on pan-European optical network for ultra-stable frequency transmissions. The experiment carried out distinct spectral dependence of amplifier gain and noise figure using standard telecom Tunable Laser pump with higher accuracy and firmware upgradation features solving the novel approach of getting an ultra-stable frequency signal gain. The approach of the make significant as the experiment carried out in C/L-Band and L-Band with complete variations of frequency characteristics occur in standard telecom.

## V. Acknowledgment

This work would not have been possible without the financial and scientific support of CESNET Optical Network Separation Department. As a main author I am grateful to work with Josef Vojtech in his busy schedule he gave me extensive professional guidance and taught me a great deal to work with Photonics. Jan Radil, Martin Slapak, Lada Altamannova, Michal Hazlinsky and Jan Kundrat had been very supportive to provide me academic time to pursue this work.

## References

[1] Shenping Li, K.S. Chiang and W.A. Gambling, “Gain Flattening of an Erbium-Doped fiber Amplifier Using a High-Birefringence Fiber Loop Mirror”, IEEE Photonics Technology Letters, Vol. 13, No. 9, September 2001. ( https://DOI:10.1364/OFC.2001.TuA5)

[2] https://czechlight.cesnet.cz/en/

[3] Josef Vojtech et.al “Alternative spectral windows for photonic services distribution”, Proc. SPIE 11128, Infrared Remote Sensing and Instrumentation XXVII, 1112806 (9 September 2019) https://doi.org/10.1117/12.2529713

[4] M.K.Dutta, “Study and Comparison of Erbium Doped Fiber Amplifier (EDFA) and Distributed Raman Amplifier (RA) for Optical WDM Networks”, 12th International Conference on Fibre Optics and Photonics 2014 , IIT Kharagpur, India , 13–16 December 2014, ISBN: 978-1-55752-882-7.

[5] http://www.id-photonics.com

[6] J.MacDonald, G.Conway, “Compensated fiber-optic frequency distribution equipment” , Proc. 42nd Annual Precise Time and Time Interval Systems and Applications Meeting, Reston, Virginia, 437-450 (November 2010)

[7] http://www.clonets.eu/clonets-posters0.html

[8] Advanced Optical Communication by Prof. R.K. Shevgaonkar, Department of Electronics & Communication Engineering, IIT Bombay.

# Precise Measuring Test Bed for Characterization of Mode Field Distribution in Different types of Multimode Fibers

J. Bohata[1,*], T. Němeček[1], M. Komanec[1], S. Zvánovec[1], P. Kormaňák[2], J. Beran[2] and J. Brouček[2]

[1]Czech Technical University in Prague, Faculty of Electrical Engineering
Department of Electromagnetic Field
Prague, Czech Republic
*bohatja2@fel.cvut.cz

[2]PROFiber Networking CZ s.r.o.
Mezi Vodami 205/29, Prague 4
Czech Republic

***Abstract*— In this paper we present experimental results from precise measurements of mode field distribution in various commercial multimode (MM) fiber types. We characterize the mode field distribution by the encircled flux (EF) parameter. EF determines optimal launch conditions in the core of the MM fiber, which is crucial especially for accurate characterizing of insertion losses at fiber connections, e.g. in data centers. For the purpose of EF measurement, a universal testbed enabling mode field characterization, integral optical power estimation or fiber connector cleanness evaluation has been proposed and experimentally verified. The uniqueness of the proposed testbed lies in backlighting of the tested MM fiber. This backlighting enables accurate positioning of the MM fiber end-face with the collimating lens to measure in the near-field area. The testbed allows the deployment of variable MM fibers and is also wavelength independent. Therefore it has the high potential within growing usage of plastic or large core fibers for short-range communications, e.g. in automotive or avionics. The obtained results are discussed within a selected real application. Moreover, since the mode field distribution is evaluated even for fibers, which do not have available any standards for EF characterization, we present new recommendations for optimal launch conditions in such fibers.**

***Keywords*— *optical fiber, multi-mode, data centers, encircled flux.***

## I INTRODUCTION

With the exponential growth of social networks, video streaming and increasing demands on data rates, the number of newly built data centers rises proportionately. It is expected in near future that 99 % of computing, storage and communication will be realized in data centers [1]. This cloud tendency contributes to the fact that the most of the data connections within data centers are shorter than 100 meters [2]. Therefore, multi-mode fiber (MMF) technology is widely deployed there reaching high bit rates in a short distance, e.g. 112 Gb/s over 100 meters of MMF while using vertical cavity surface emitting laser (VCSEL) [3]. Despite discussions about potential single mode fiber (SMF) deployment in data centers, MMFs and MMF components will still be dominant in the future [4], [5]. Together with considering data volume growth, MMF network proper characterization deserves increased attention.

The high bit rate connections in data centers have special limits for power budget and insertion losses (IL). However, the IL measurements can be quite different for various optical sources. Whereas lasers (mostly VCSEL) are highly collimated and tend to produce under-filled launch (UFL) conditions, the light-emitting diodes (LEDs) produce typically overfilled launch (OFL) conditions with a higher number of excited and guided modes [6]. The UFL is then more sensitive to small variations in the MMF´s refractive index profile and the IL measurements with UFL can give more optimistic results than further experienced in a real network, especially for fiber connections. On the other hand, MMF with strong OFL shows significantly higher IL [7].

Furthermore, analyses of two MMFs with increasing transverse offset error in [2] revealed that optical power coupled from the lowest order mode [8] dramatically decreases while the total coupled power to the fiber is in this case transferred to the higher order modes. We have investigated MMF connection imperfections for aircraft MMF network under temperature and vibrational conditions in detail in [9] and revealed that transverse offset of the MMF in adapters due to vibrations results in a significantly higher number of guided modes and decreased transmission bandwidth due to differential mode delay (DMD). Moreover, an optimal-filled launch light was required in such a network. For this reason, the encircled flux (EF) definition has been adopted as a measure for MMF component characterization [10], [11], [12]. The EF parameter determines optimal-filled

launched to MMF core, with precisely set required limits between UFL and OFL. Multi-mode links can be parametrized by sources fulfilling EF requirements to correctly evaluate IL [13], [14]. For this reason, all utilized equipment must fulfill EF conditions. Last but not least, the EF measurement introduces a better understanding of guiding conditions in MMF and standardizes MMF components.

However beside classical communication MMF with graded-index profiles with 62.5 and 50 µm cores with latest standard of OM5 [15], optical fibers with SI profile have attracted attention recently, especially in automobile industry. According to the standardization organization for media oriented systems transport (MOST), more than 204 carmakers including Volvo, BMW, Audi, Mercedes, and Cadillac are now using step-index-plastic optical fiber SI-POF as a physical medium for automobile networking [16]. Moreover, for home networking applications, current effort including the Europe Union project initiative POF-Plus is to standardize a 1 Gbps link over 50 m of 1 mm SI-POF [17]. Therefore, there have been published several papers investigating modal power distribution (MPD) in SI, i.e. plastic, fibers [18], [19], [20], [21].

Nevertheless, above mentioned papers presented a far-field angular EF characterization for SI fibers instead of near-field EF characterization given by standard IEC61280 for telecommunication fibers. In this paper, we show analyzer of mode structure of optical components, realized in project from Ministry of Industry and Trade of Czech Republic, for different types of MMF to characterize EF parameter to evaluate MPD for various applications with core size from 50 to 980 µm.

## II TESTBED DESCRIPTION & RESULTS

The proposed testbed is based on scheme shown in Fig. 1. For precise measuring of MPD for both graded- and tep-index fibers, the analyzer is composed from fiber´s end-face holder, mounted on micromovement stage, which accurately places the end-face, i.e. optical connector, to appropriate position against aspheric lens. The aspheric lenses are commonly used when the incoming beam is to be between one and five millimeters since aspheric lenses do not introduce spherical aberration. The aspheric lens then ensures collimation of the beam to capture signal in near-filed profile, according to the standards. The collimated beam then propagates through 50/50 beam splitter from which 50 % of the signal is led toward camera, i.e. a CMOS or CCD sensor. This way the signal from testing fiber with particular optical source is captured by sensor and analyzed in proposed program called Avisok. For large core fibers (over 250 µm core diameter), another plano-convex lens is used to

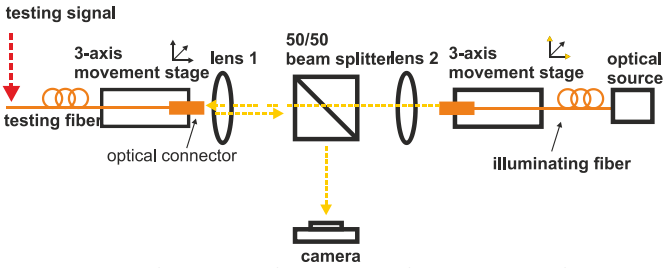


Fig. 1. Simplified scheme of the analyzer of mode structure of optical components.

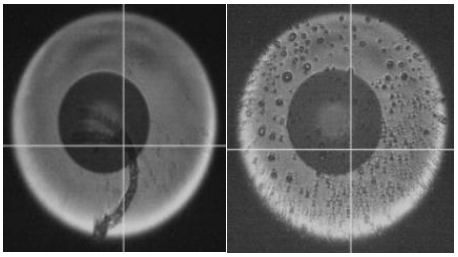

a)

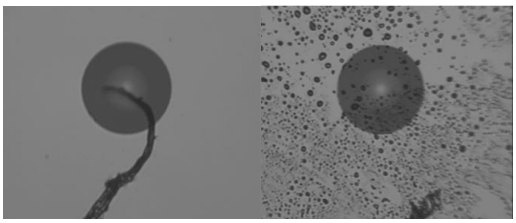

b)

Fig. 2.a) analysis of the OM3 connector dirtiness for a) proposed analyzer and b) fiber inspection probe EXFO FIP 420-B.

diminish the incoming beam due to small size of the sensor chip. However, in order to calibrate the system for precise measurement, it is necessary to determine the magnification of the testbed, in particular because of using couple of optical components changing size of the objects displayed by sensor and moving of fiber´s end-face to find right focal distance. Therefore, a reverse illuminating is used by the source at the same wavelength as using by tested components. The beam is launched from standard graded-index MMF connector and further broadened by biconvex lens to fully cover testing connector. Then the illuminating signal is split by the splitter,

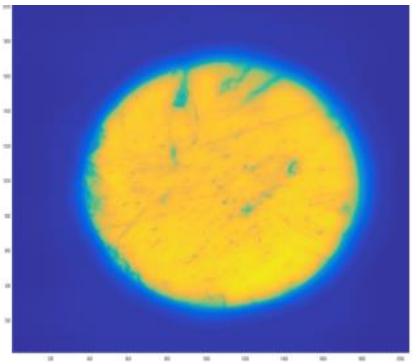

a)

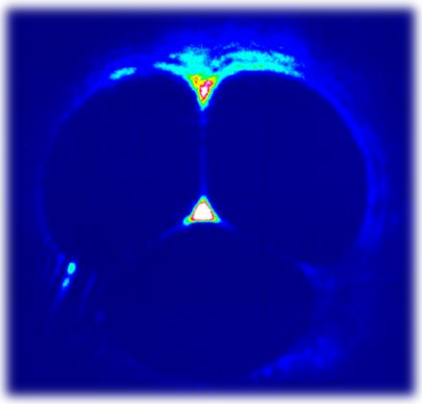

b)

Fig. 3. Opposite illuminating of a) POF with 486 µm core diameter and b) microstructure fiber.

reflected from the testing connector and travel at the same way like testing beam to sensor. Note that this is done at the beginning of the measurement to check the cleanness of the connector and calibrate setup from known diameter of the fiber core. The evaluation of the dirtiness of the OM3 connector for the proposed analyzer is shown in Fig. 2, compared with commercially available fiber scope (EXFO FIP 420-B). This analysis serves to check conditions of the connector and also, as mentioned above, to system calibration. Besides common communication MMFs, also special fibers can be used as shown in Fig. 3 for e.g. SI-POF or microstructured optical fiber making the system universal.

Moreover, the system is capable after calibration to determine power launching form testing fiber with accuracy better than -+ 1mW. Also the testbed is universal due to wide range of wavelengths by the especially change of sensor and eventually the other optical components. Thus the system can be easily designed for multiple wavelengths used in telecommunications, i.e. 850, 1310 and 1550 nm. Another key assumption for accurate evaluation of MPD is appropriate camera setting with correct gain and exposition. Fig. 4 depicts power distribution in POF with 486 µm core diameter for different setting of exposure time. Yellow and green curves represent x- and y-axis cuts. Note that optical source was a halogen lamp (Ocean optics HL-2000). It is shown how the beam spot and also x and y profiles changes according to exposure time from over-exposed (top left) to under exposed (bottom right). The ideal exposition is in this case the middle right picture where the high dynamic range is maintained and no information is lost due long exposure time.

Next, the EF parameter, measured in near-filed, for different MMF with various core diameter has been evaluated. Note that EF is defined by IEC standard wit following equation [11], [12]:

$$EF(r) = \frac{\int_0^r xI(x)dx}{\int_0^R xI(x)dx} \quad (1)$$

The proposed testbed has been compared for commonly used fibers with core diameters of 50 and 62.5 µm with results obtained from the calibrated EF-meter (Arden Photonics MPX-1). Results from measurements with superluminescent diode (SLED) optical source are depicted in Fig. 5. Whereas EF points, measured by MPX-01 are indicated by red dots, EF points

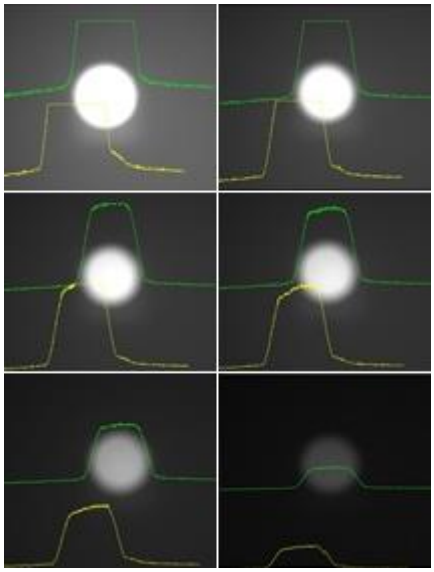

Fig. 4. Different exposure times for MPD of POF with 486 µm core diameter.

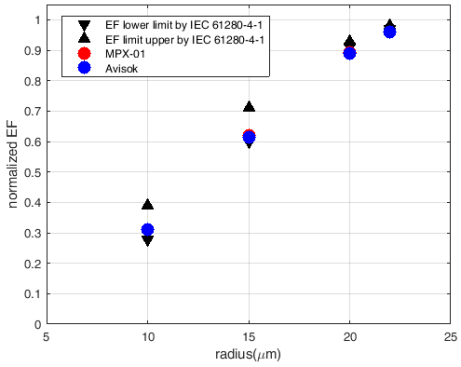


a)

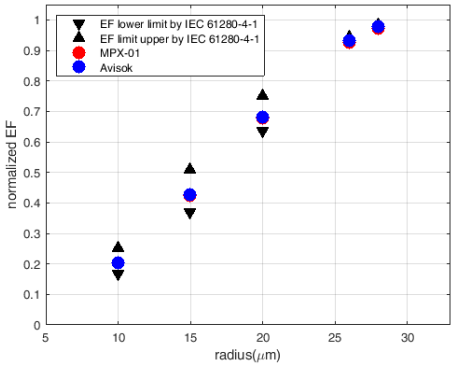


b)

Fig. 5. Comparison of obtained EF results between our testbed (Avisok - blue) and reference on (Arden Photonics MPX-1 - red) for fiber core diameters a) 50 µm and b) 62.5 µm.

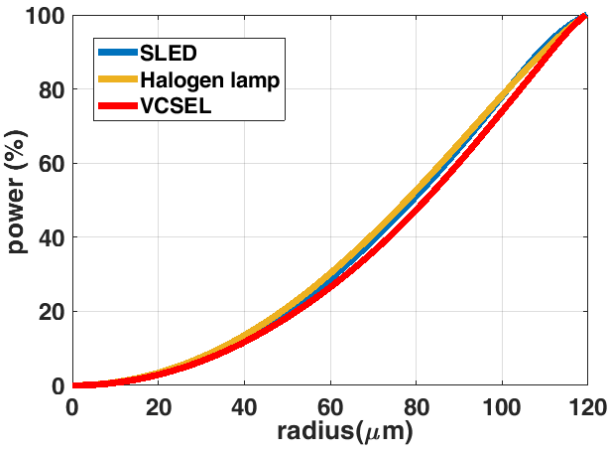


Fig. 6. EF performance in POF with core size of 240 µm for SLED (blue), Halogen lamp (yellow) and VCSEL (red) optical sources.

obtained by Avisok analyzer are indicated by blue dots. Upper and lower limits given by standard IEC61280-4-1 are represented by triangle markers. It can be clearly seen that there is perfect agreement with both measured profiles showing only negligible differences, which are caused by instable modal conditions in tested fibers. However, the maximal core diameter, which is possible to measure in MPX-01, is 100 µm. Therefore we have used only Avisok for measurement of special large-core optical fibers such as POF or plastic-clad silica (PCS) fibers.

At first, an EF for POF with 240 µm core diameter has been evaluated for different optical sources, namely SLED, halogen lamp and vertical-cavity surface-emitting laser (VCSEL). Note

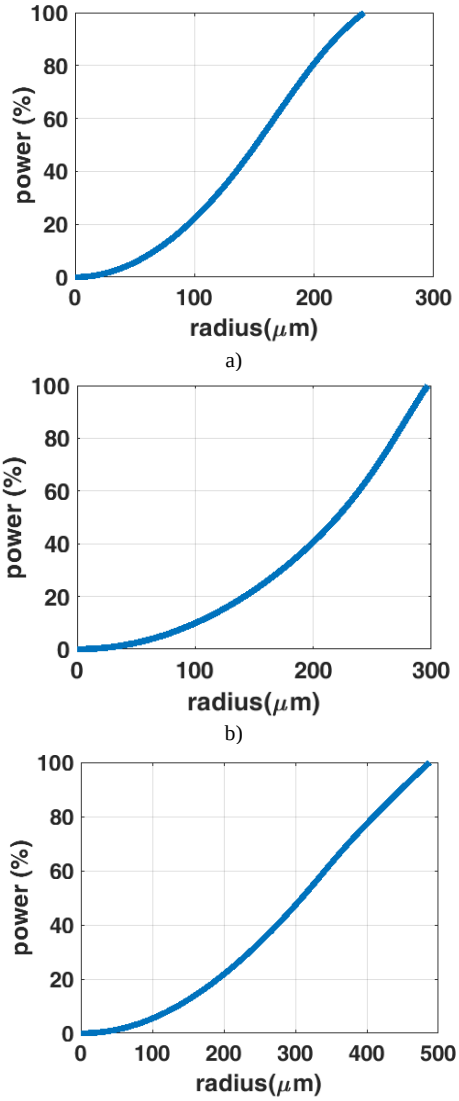


Fig. 7. EF profiles for a) POF with core diameter of 486 µm, b) PCS fiber with core diameter of 600 µm and c) POF with core diameter of 980 µm.

that whereas halogen lamp is extremely broadband (λ ~ 360 – 2400 nm), SLED and VCSEL have their maximal output power at 850 nm. As implied from Fig. 6, the MPD is almost independent on type of the source for SI, i.e. POF, fibers, comparing to graded-index MMF. Nevertheless, the system is capable to reveal potential inhomogeneity or measure mode field diameter. Finally, three types of large-core fibers, i.e. POF with core diameters of 486 µm and 980 µm and PCS with core diameters of 600 µm have been measured in terms of their EF performance. In this case, the laser source was halogen lamp. Results are shown in Fig. 7. The POFs exhibit almost linear filling of the core except of first quarter, where is more exponential. On the other hand, the PCS fiber curve is similar to exponential shape in whole range. No EF target is displayed since there are no specifications for optimal large-core fibers filling.

## III SUMMARY

A universal analyzer for MPD evaluating EF parameter for wide range of optical wavelengths and various types of optical fibers with different core size has been presented. We demonstrated its functionalities useful for characterizing of variable MMF used for e.g. datacenters or automotive industry. These functionalities involve fiber connector inspection, optical power estimation, mode field diameter measurement and in particular MPD characterization in terms of EF. Moreover, the accuracy of proposed testbed was successfully verified by commercially available reference meter. Finally, the EF parameter was evaluated for optical fibers with SI refractive profile with core size from 240 to 980 µm and the impact of variable optical sources for such fibers was determined.

## ACKNOWLEDGMENT

This work has been supported by the project of the Ministry of Industry and Trade, TRIO FV10519.

## REFERENCES

[1] A. Vahdat, "Delivering scale out data center networking with optics — Why and how " in OFC/NFOEC, pp. 1-36, 2012.

[2] W. V. Sorin and M. R. Tan, "Interoperability of single-mode and multimode data links for data center and optical backplane applications," in OFC/NFOEC, pp. 1-3, 2013.

[3] F. Karinou, N. Stojanovic, C. Prodaniuc, Z. Qiang and T. Dippon, "112 Gb/s PAM-4 optical signal transmission over 100-m OM4 multimode fiber for high-capacity data-center interconnects," in 42nd European Conference on Optical Communication (ECOC), pp. 1-3, 2016.

[4] D. Mahgerefteh, C. Thompson, C. Cole, G. Denoyer, T. Nguyen, et al., "Techno-economic comparison of silicon photonics and multimode VCSELs," J. Lightwave Technol., vol. 34(2), pp. 233-242, 2016.

[5] J. A. Tatum, D. Gazula, L. Graham, J. Guenter, R. H. Johnson, J. King, et al., "VCSEL-based interconnects for current and future data centers," J. Lightwave Technol., vol. 33(4), pp. 727-732, 2015.

[6] C. DeCusatis and I. Kaminow, The optical communications reference: Elsevier Science, 2009.

[7] M. J. Hackert, "Explanation of launch condition choice for GRIN multimode fiber attenuation and bandwidth measurements," J. Lightwave Technol., vol. 10(2), pp. 125-129, 1992.

[8] M. B. Shemirani, W. Mao, R. A. Panicker and J. M. Kahn., "Principal modes in graded-index multimode fiber in presence of spatial- and polarization-mode coupling," J. Lightwave Technol., vol. 27(10), pp. 1248-1261, 2009.

[9] J. Bohata, M. Pisarik, S. Zvanovec and P. Peterka, "Reliability of aircraft multimode network," Opt. Eng. vol. 53(9), 2014.

[10] G. He, M. Breton, S. D. Poirer, G. Bull, G. W. Schin, Y. St-Amant, et al., "Improved near-field scanning system for encircled flux measurement," IET Optoelectron., vol. 5(1), pp. 46-49, 2011.

[11] International standard "IEC 61280-4-1 Ed. 2.0, Fibre-optic communication subsystem test procedures – Part 4-1: Installed cable plant – multimode attenuation.measurement", 2009.

[12] International standard, "IEC 61280-1-4 Ed. 2.0: Fibre-optic communication subsystem testprocedures – Part 1-4: General communication subsystems – lightsource encircled flux measurement method", 2009.

[13] S. Kobayashi and O. Sugihara, "Encircled Angular Flux: A new measurement metric for radiating modal power distributions from step-index multimode fibers," J. of Lightwave Technol., vol. 34(16), pp. 3803-3810, 2016.

[14] M. Kagami, A. Kawasaki, M. Yonemura, M. Nakai, P. V. Mena and D. R. Selviah, "Encircled angular flux representation of the modal power

distribution and its behavior in a step index multimode fiber," J. of Lightwave Technol., vol. 34(3), pp. 943-951, 2016.

[15] E. R. Parsons, R. Patterson, J. Young and P. F. Kolesar, "The Impact of Effective Modal Bandwidth on 100G SWDM Transmission Over 250 m OM5 and Left-Tilt OM4 Multimode Fibers," in J.l of Lightwave Technol. vol. 36, no. 24, pp. 5841-5848, 2018.

[16] N. A. Albakay and L. Nguyen, "Achieving 1 Gbps Over Step-Index Plastic Optical Fiber Using Spatial Mode Air-Gap Filter," in IEEE Photon. Technol. Lett., vol. 29, no. 8, pp. 655-658, 2017.

[17] C. M. Okonkwo et al., “Recent results from the EU POF-PLUS project: Multi-gigabit transmission over 1 mm core diameter plastic optical fibers,” J. Lightw. Technol., vol. 29, no. 2, pp. 186–193, Jan. 15, 2011.

[18] S. Kobayashi and O. Sugihara, "Encircled Angular Flux: A New Measurement Metric for Radiating Modal Power Distributions from Step-Index Multimode Fibers," in Journal of Lightwave Technology, vol. 34, no. 16, pp. 3803-3810, 15 Aug.15, 2016.

[19] M. Kagami, A. Kawasaki, M. Yonemura, M. Nakai, P. V. Mena and D. R. Selviah, "Encircled Angular Flux Representation of the Modal Power Distribution and Its Behavior in a Step Index Multimode Fiber," in Journal of Lightwave Technology, vol. 34, no. 3, pp. 943-951, 1 Feb.1, 2016.

[20] S. Kobayashi, K. Horiguchi, Y. Hyakutake and O. Sugihara, "Evaluation of Modal Power Distribution of Automotive Optical Gigabit Ethernet Connections," in Journal of Lightwave Technology, vol. 35, no. 17, pp. 3664-3670, 1 Sept.1, 2017.

[21] M. Kagami, A. Kawasaki and M. Yonemura, "Modal power distribution in short reach optical communications using step-index-type multimode optical fibers," 2013 3rd IEEE CPMT Symposium Japan, Kyoto, 2013, pp. 1-4.